A spectral method aimed at explaining the role of the heat transfer rate when the Infinite Line Source model is applied to Thermal Response Test analyses

Stefano Morchio[a] Philippe Pasquier[b] Marco Fossa[a] Richard A. Beier[c]

a- Dime Department of Mechanical, Energy, Management and Transportation Engineering, The University of Genova, via Opera Pia 15, 16145 Genova, Italy
b- Department of Civil, Geological and Mining Engineering, Polytechnique Montréal, C.P. 6079 Succ. Centre-Ville, Montréal, Québec, Canada H3C 3A7
c- Division of Engineering Technology, Oklahoma State University, Stillwater, OK 74078, USA

ABSTRACT

The present paper introduces new concepts related to the modeling of vertical Borehole Heat Exchangers for Ground Coupled Heat Pump applications. A sensitivity analysis on how specific parameters affect the ground thermal conductivity k_{gr} estimation when the Infinite Line Source model is used to interpret a Thermal Response Test has been performed. The study has been conducted considering shallow and deep BHEs, with and without geothermal gradient, and for homogeneous and stratified ground thermal conductivities. The q_{ratio} parameter scales the external heat rate to a natural heat rate associated with the geothermal gradient. The effect of q_{ratio} on the TRT analysis has been related to a specific dimensionless g-transfer function called $g_{0,}$ which incorporates the geothermal gradient. Three in-house built Fortran90 codes implementing the finite-difference models related to coaxial, single and double U-BHE geometries are exploited to evaluate the dimensionless g-transfer functions related to each fluid volume. A spectral method aimed to reconstruct the fluid temperature profiles by superposing two separated convolutions in the time domain exploiting the Fast Fourier Transform leads to considering q_{ratio} as the dominant parameter when the ILS model is used to estimate k_{gr}. In the case of a single-layered subsurface, q_{ratio} >>1 guarantees the correct ILS-based k_{gr} estimation for any BHE geometry. In the coaxial center-pipe inlet case with a single-layered subsurface and q_{ratio}<1, the ILS-based k_{gr} estimation when the g_0-function is taken into account can differ by -14 % from the correct ILS-based k_{gr} estimation without taking into account the g_0-function. In the case of a multilayered subsurface, the q_{ratio} parameter indicates when the

S. Morchio (stefano.morchio@edu.unige.it) is PhD student at DIME Dept., University of Genova, Italy, and visiting student at Polytechnique Montréal, Canada in 2022
P. Pasquier (philippe.pasquier@polymtl.ca) is Full Professor at Polytechnique Montréal, Canada
M. Fossa (marco.fossa@unige.it) is Full Professor at DIME Dept., University of Genova, Italy
R. A. Beier (rick.beier@okstate.edu) is Professor Emeritus, Oklahoma State University, Stillwater, OK, USA

effective k_{gr} estimated by the ILS model departs from the weighted-thickness average. A departure of 10% occurs for q_{ratio} between 2 and 2.5 for the coaxial center-pipe inlet cases considered and the departure increases with decreasing q_{ratio}.

Key Words: thermal response test, spectral method, short-term *g*-function, deep borehole heat exchanger, ground thermal conductivity, geothermal gradient

NOMENCLATURE

b	constant [K]
c	specific heat [J/kg K]
E_1	exponential integral in ILS model [-]
Fo	Fourier number [-]
FFT	Fast Fourier Transform
f	external excitation function [°C]
g	dimensionless temperature transfer function [-]
H	active depth of the BHE [m]
k	thermal conductivity [W/(m·K)]
m	slope [K/cycles]
$\dot{m}$	mass flow rate [kg/s]
n_t	number of elements of the solution related to the temporal discretization
N_1	net transfer unit corresponding to short-circuit heat transfer (coaxial) [-]
N_2	net transfer unit corresponding to heat transfer between fluid and ground (coaxial) [-]
N_{gr}	dimensionless conductance of ground [-]
$\dot{Q}$	heat transfer rate [W]
$\dot{Q}'$	heat transfer rate per unit length [W/m]
$\dot{Q}''$	heat flux rate [W/m^2]
q_{ratio}	ratio of external heat input rate per unit length to an idealized (natural) heat rate [-]
R	thermal resistance [m·K/W]
r	radial coordinate [m]
S	temperature profiles from numerical solution (or experimental measurements) [°C]
T	temperature [K]
w	velocity [m/s]
z	vertical coordinate [m]

Greek letters

α	thermal diffusivity [m^2/s]
β	dimensionalization constant of the spectral method [°C]
γ	Euler constant [-]
ρ	density [kg/m^3]
Δ	finite increment in a variable [-]
π	pi constant [-]

τ	time [s]

Subscripts

ave	average
b	borehole
f	heat carrier fluid
geo	geothermal
gr	ground
in	inner dimension/inlet
j	index, spatial discretization (vertical)
out	outlet dimension/outlet
p	index, ground layer
∞	far field and initial condition
0	initial condition

Superscripts

n	index, temporal discretization
*	effective

1. Introduction

As reported by the International Energy Agency (IEA) [1], Ground-Coupled Heat Pumps (GCHP) are indicated as the most effective system (in terms of energy savings and reductions in CO_2 and greenhouse gas emissions) for efficient heating, ventilation, and air conditioning of buildings for civil and industrial use. In most European countries, heating, and air conditioning of buildings accounts for nearly 50% of total primary energy consumption [2]. The high energy efficiency guaranteed by the GCHP makes these systems increasingly attractive for the suitable air conditioning of buildings. GCHP systems are constituted by a heat pump coupled with the ground through multiple vertical or horizontal ground heat exchangers. Vertical borehole heat exchangers (BHEs) represent the most frequent solution adopted. The borehole depth related to conventional BHEs is frequently 200 m or less.

As highlighted by several studies, such as the one by Holmberg et al. [3], when the BHEs overcome the depth of 350 m (the typical limit for air drilling) these are referred to as Deep Borehole Heat Exchangers (DBHEs). Drilling at such a large depth (even more than 800–1000 m) has the great advantage of exploiting higher temperature levels, especially if the ground has a significant geothermal gradient. In such a way, the surface extension for drilling is reduced together with the total pipe length, making the DBHEs economically the better choice for supplying heat to an entire urban district. Larger depths are attractive, especially for buildings requiring high heat loads in densely populated and cold urban areas, as highlighted by Morchio and Fossa [4]. Several authors, such as Deng et al. [5], highlight how the coaxial (pipe-in-pipe) is the usual geometry employed for DBHEs. Hellström [6] and Acuña [7] report that the coaxial arrangement makes the thermal and hydrodynamic performance of the BHEs better than those obtainable with U-tubes. In addition, the coaxial geometry represents the most suitable solution for its intrinsically easier installation procedure at the typical depths of DBHEs, as described by Acuña [7]. As in the previous study by Morchio et al. [8], the thermal transient behavior of coaxial DBHEs is numerically simulated and compared with the one related to single and double U DBHEs. The circulation profiles resulting from the simulations reported in the present paper confirm once more and portend the thermal benefits guaranteed by the coaxial geometry for DBHE applications in both the heat injection and extraction operation mode in comparison with those provided by U-pipes.

The sizing of GCHP systems requires the most accurate knowledge of the ground thermal properties. In particular, the ground thermal conductivity k_{gr} and its variation along with depth are of primary importance for the correct sizing and selecting the most cost-effective depth for a borehole field. Thermal response tests (TRT) constitute the usual experimental procedure to be performed by exploiting a pilot BHE already installed in order to estimate the ground thermal conductivity and borehole thermal resistance. The TRT experimental technique and the related equipment were introduced by the pioneering work of Mogensen [9]. Different typologies of setup and measurement techniques (first of all the Distributed Thermal Response Test, DTRT) have been proposed throughout the years by different Authors [10,11,12,13,14,15,16,17,18]. The study by Galgaro et al. [19] demonstrates how the most relevant lithological thermal parameters as the equivalent k_{gr} of the entire stratigraphy and also the k_{gr} related to each layer with a spatial resolution of 1 m can be obtained thanks to the temperature measurements collected from the optical fiber cable actively heated by a constant heating power injected through copper wires contained within the cable structure.

In the present paper three Fortran90 programs implementing the finite-difference (FD) models related to coaxial, single and double U BHEs presented in previous investigations by the present research group [4,20,21] have been exploited for evaluating the influence of specific TRT parameters on the ground thermal conductivity estimation when the First Order Approximation (FOA) of the Infinite Line Source (ILS) model by Carslaw and Jaeger [22] is applied in TRT analysis. The simulated cases reported in the present study are addressed to evaluate the influence of these parameters for shallow and Deep BHEs penetrating a single or multiple ground layers with different geothermal gradients imposed along the depth.

A previous study by Liu et al. [23] highlights how the layered subsurface and geothermal gradient have a great impact on the heat extraction performance of a medium-deep borehole heat exchanger. The weighting factors on individual-layer properties proper of the layer-factor method developed by Beier et al. [24] reveal how conventional 1D models determine the effective ground thermal conductivity in simulated DTRTs in deep boreholes. The weighting factors change with heat injection versus heat extraction, placement of the fluid inlet, and the direction of increasing ground thermal conductivity. The studies by [25,26,27,28] found that the ILS-based k_{gr} estimated value is near the weighted-thickness average. It has to be taken into account that these last studies together with those numerical and experimental by [29,30,31,32,33,34] on TRT and DTRT analyses were focused on shallower boreholes (depth < 150 m).

Beier [35] developed a 2D heat transfer model of coaxial DBHEs (depth > 350 m) able to highlight how the geothermal gradient affects TRT estimates of ground thermal conductivity. The study by Beier et al. [36] was focused on performing DTRT analyses through numerical models for coaxial DBHEs to study the effect of upward and downward increasing trends of thermal conductivity among ground layers on the estimate of the mean k_{gr} and the k_{gr} estimates for individual layer.

The present study extends the analyses of simulated TRT and DTRT involving single and multiple layers with a constant (or variable with depth) and positive geothermal gradient considering coaxial, single and double U DBHEs. Among the different parameters investigated, the present study highlights the effect of the q_{ratio} parameter introduced by Morchio et al. [8] on the ground thermal conductivity estimation when the conventional-1D ILS model is applied to interpret the TRT data. The q_{ratio} parameter is defined as the ratio between the absolute value of the external heat transfer rate $\dot{Q}'$ (per unit length) and what we call the natural heat rate $\dot{Q}'_{geo}$ that corresponds to the vertical geothermal flux multiplied by the BHE length. As it is easy to deduce, the heat available in the ground can be favorably exploited by DBHEs. In DBHEs, the influence of the heat injected/extracted rate on the estimated value of the ground thermal conductivity from a TRT can occur through the interaction between the injected/extracted heat rate and the natural geothermal gradient. As the borehole depth increases, more importance is assumed by the q_{ratio} parameter. This implies that during the planning and the execution of a TRT, especially when DBHEs are involved, it should be highly recommended to have performed and made available the undisturbed ground temperature profile measurements, like those provided by Holmberg et al. [37] to have an estimate of $\dot{Q}'_{geo}$. In this manner, the engineer can choose the more suitable heat transfer rate $\dot{Q}'$ to apply to the carrier fluid during the TRT, thus controlling and in case modifying q_{ratio}. The simulations' results reported in the present paper verify that q_{ratio} is the dominant parameter that indicates when the ILS-based k_{gr} estimated value departs from the weighted-thickness average.

In addition, the present study is aimed to highlight how the effect of the q_{ratio} parameter on the TRT analyses is also related to a specific dimensionless g-transfer function called g_0 that is obtained by performing a complete circulation test of the same duration of the TRT. The dimensionless temperature transfer functions (Temperature Response Factor) and the related approach of the g-functions are credited to Eskilson [38]. Further developments for their convolutions performed in the spectral domain are due to Pasquier and Marcotte [39,40,41]. The g_0 function incorporates the geothermal gradient and in general, the disturbance effect (particularly prominent for DBHEs) related to the undisturbed ground temperature profile during the TRT. One of the aims of the present study is to demonstrate that when q_{ratio} is lower than 1 the $g_{0,j}(\tau)$ function is able to modify the slope of the general solution $T_{f,j}(\tau)$ for each fluid node.

2. Theory and insights on q_{ratio} parameter and the g-transfer functions in TRT analysis

The TRT is the experimental technique aimed at obtaining an estimate of the ground thermal conductivity k_{gr} and the effective borehole thermal resistance R^*_b. The accurate knowledge of k_{gr} is crucial for the correct sizing of the BHE field. Usually, the test is performed by measuring the heat carrier fluid temperatures in a pilot BHE, according to the method introduced and described by Mogensen [9]. The TRT setup consists of an electric heater equipped with temperature sensors at the inlet and the outlet sections (temperature measurements of the carrier fluid), a circulation pump, a flow meter and the closed-loop piping in the borehole. The prior circulation phase of the test, without injecting or extracting any heat, is aimed to reach the thermal equilibrium between the fluid and the surrounding ground. The circulation phase is followed by the heat injection (or heat extraction) phase during which the carrier fluid flow is constantly heated (or cooled) by the TRT machine. In this manner, the heat transfer rate exchanged by the fluid flowing in the BHE closed-loop causes a thermal interaction with the surrounding ground. Analyzing the thermal response measurements consequent to this interaction allows for estimating the ground thermal conductivity k_{gr}. Among the different models that can be applied, the ILS model [22,42] is the first and the simplest for estimating k_{gr}. More details on the ILS-based analysis of the TRT data are provided in Appendix A.

The k_{gr} estimated value by applying the ILS model in the TRT analysis in cases of single and multiple layers is an effective value of the ground thermal conductivity. This value is near the weighted-thickness average, as confirmed by previous studies focused on shallower boreholes (depth < 150 m) by [25,26,27,28]. For layered ground, the average is the effective ground thermal conductivity for parallel heat conduction through layers with boundary conditions of uniform temperature at each end. Thus, the weighted average is a useful reference value. In the case of layers with equal thickness, the average is the simple arithmetic mean.

Except for the first 20 m of the substrate that is subjected to seasonal temperature oscillations, the ground temperature approximately increases linearly with depth, according to a geothermal gradient generally in the 0.02-0.03 K/m range. The ground temperature behavior can be well described by the Lunardini [45] analytical solution. Quite rare "geothermal anomalies" (due to surface magma chambers) and the presence of deep water-saturated soils are the exceptions to the above rule. In TRT and GCHP applications, the importance assumed by the q_{ratio} parameter increases, according to its definition, as the borehole active depth H increases:

$$q_{ratio} = \frac{\frac{\dot{Q}}{H}}{k_{gr} H \frac{dT_{gr,\infty}}{dz}} \quad (1)$$

where $\dot{Q}/H$ is the external heat rate per unit length while the denominator represents the natural heat rate $\dot{Q}'_{geo}$ corresponding to a constant geothermal gradient, $dT_{gr,\infty}/dz$, and defined as:

$$\dot{Q}'_{geo} = k_{gr} H \frac{dT_{gr,\infty}}{dz} \quad (2.1)$$

Under the assumption of a constant geothermal heat flux through the ground layers, Fourier's law of heat conduction allows to express the density of natural heat flux $\dot{Q}''_{geo}$ as the product between the layer ground thermal conductivity, $k_{gr,p}$ and the temperature gradient, $(\frac{dT_{gr,\infty}}{dz})_p$, of each layer proper of the undisturbed ground:

$$\dot{Q}''_{geo} = k_{gr,p} (\frac{dT_{gr,\infty}}{dz})_p \quad (2.2)$$

As observed by Raymond [46], Eq. (2.2) does not always apply especially for depths less than 50 m. It has to be taken into account, as noticed by Kohl [47,48] and Huang et al. [49], that palaeoclimatic temperature signals in the subsurface and the impacts of urbanization can produce significant deviations from steady-state undisturbed ground temperature profiles given by Eq. (2.2). Even though the above mechanisms can move profiles from the steady-state profile corresponding to a constant geothermal heat flux, Eq. (2.2) confers a good approximation of the real profile for identifying the overall thermal condition of the ground (especially when high depths proper of Deep BHEs are reached) and is still useful to represent overall trends.

The ILS model assumes the heat transfer rate per unit length injected (or extracted) by the carrier fluid to (from) the surrounding ground (across the borehole wall) uniform with depth. In the present study, the effect due to a linear undisturbed ground temperature profile that increases with depth since characterized by a constant geothermal gradient has been numerically investigated. This linear temperature profile has been assumed for simplicity (and also because this represents a good approximation of the realistic profile proper of Deep BHEs). It can be expected that the uniform-flux assumption proper to the ILS model eventually breaks down with increasing geothermal gradient and/or increasing borehole depth. In this case, as stated by Morchio et al. [8], the natural heat rate corresponding to the geothermal gradient can change the heat flux normally imposed by the external heat rate during a TRT causing competition between the two heat rates of different origins (the external heat injection/extraction rate and the natural heat rate). The typical depth H reached by the DBHEs allows the exploitation of the natural heat $\dot{Q}'_{geo}$ made available at such depths. In particular, the thermal performance and the heat transfer rate that can be extracted by the DBHEs for GCHP applications are enhanced as the $\dot{Q}'_{geo}$ is higher, as shown by previous studies by [3,8]. On the other hand, as highlighted by Morchio et al. [8], the k_{gr} estimated value from an ILS-based TRT analysis can be highly influenced by the q_{ratio} parameter. This is because as the borehole active depth H increases, the thermal interaction between the external injected/extracted $\dot{Q}/H$ and the natural $\dot{Q}'_{geo}$ increases. The numerical results related to the simulations reported in the present paper for a single and a multilayered subsurface of different k_{gr} values lead to understanding and verifying that q_{ratio} is the dominant parameter that indicates when the ILS-based k_{gr} estimated value departs from the weighted-thickness average. One of the main assumptions of the ILS model is that a constant heat transfer rate in time and space is irradiated (or absorbed) from a linear source embedded into a medium of infinite extent. According to Pasquier and Marcotte [40], if the heat flux signal is of step function type varying with time, the temporal superposition principle can be used to express the temperature variation at any time $\tau=\tau_{n_t}$, where n_t is the number of previous time steps:

$$T(r,\tau) - T_{gr,\infty} = \sum_{n=1}^{n_t} \frac{\dot{Q}'_n - \dot{Q}'_{n-1}}{4\pi k_{gr}} \int_{\frac{r^2}{4\alpha_{gr}(\tau-\tau_{n-1})}}^{\infty} \frac{e^{-\beta}}{\beta} d\beta; \qquad \tau_{n_t-1} < \tau \leq \tau_{n_t} \tag{3}$$

which can be rewritten, for each j_{th} node of the fluid domain, as:

$$T_{f,j}(\tau) - T_{gr,\infty} = \sum_{n=1}^{n_t} f(\tau_n) g_j(\tau - \tau_{n-1}) \tag{4}$$

where

$$f(\tau_n) = \dot{Q}'(\tau_n) - \dot{Q}'(\tau_{n-1}) \tag{5}$$

and

$$g_j(\tau-\tau_{n-1}) = \frac{1}{4\pi k_{gr}}\int_{\frac{r^2}{\frac{4\alpha_{gr}}{\tau-\tau_{n-1}}}}^{\infty} \frac{e^{-\beta}}{\beta} d\beta \quad (6)$$

Therefore, according to Pasquier and Marcotte [40], the ILS model can be decomposed into an incremental heat flux function f and a model-specific integral g_j evaluated for a constant and unit heat pulse [39] for each j_{th} node, see Eqs. (4), (5), (6). Computing Eq. (4) in the time domain for a long heat flux signal $\dot{Q}'$ is computationally intensive. Marcotte and Pasquier [39] noticed that the right-hand side of equation (4) corresponds to a convolution product, noted $(f*g_j)(\tau)$, and suggested solving it by using a spectral approach. This means that being the convolution in the time domain corresponding to multiplication in the frequency domain, $(f*g_j)(\tau)$ is connected to discrete Fourier transforms. Denoting with the letter F the Fast Fourier Transform (*FFT*) and F^{-1} the Inverse Fast Fourier Transform (the symbols "*" and "·" in Eq. (7) are the symbols related to the convolution product and the Hadamard product respectively) any convolution $(f*g)(\tau)$ in the time domain can be computed exploiting the frequency domain according to the following general expression:

$$(f * g_j)(\tau) = F^{-1}(F(f) \cdot F(g_j)) \quad (7)$$

According to Pasquier and Marcotte [40], the spectral approach to solve a convolution product by *FFT* can be exploited under the following main assumptions:

- The heat flux signal is represented by a step function.
- All the heat pulses are of equal duration ($\Delta\tau=\tau_j-\tau_{j-1}$).
- f and g_j (f_0 and $g_{0,j}$) are both periodic functions.

In case one or both f and g_j (f_0 and $g_{0,j}$) are not periodic functions, the zero-padding technique can be adopted, as reported by Pasquier and Marcotte [40]. The zero-padding technique consists in adding n_t - 1 zeros at the end of vectors f and g_j, to evaluate $F^{-1}(F(f) \cdot F(g))$ with these zero-padded vectors, and then to keep only the first n_t elements of the solution.

The solution provided by Eq. (7) gives the temperature change with respect to zero, as the ground (and the carrier fluid) is uniformly at 0°C as the initial condition. According to Pasquier and Marcotte [40], to reconcile the real ground temperature with Eq. (7), the temperature at any node is simply given by Eq. (8):

$$T_{f,j}(\tau) = (f * g_j)(\tau) + T_0 \quad (8)$$

where T_0 is the mean initial undisturbed ground temperature. Eq. (8) assumes a uniform ground temperature profile over the domain's height. It is important to highlight that Eq. (8) assumes a uniform ground temperature profile T_0 over the domain's height (a zero geothermal gradient). The present study considers that a real vertical thermal profile data set is available and the geothermal gradient is taken into account. This generalization is provided by Eq. (9). According to Pasquier and Marcotte [40,41] the numerical (or experimental) temperature profiles $S_j(\tau)$ resulting from a series of heat pulses can be reconstructed by the general solution $T_{f,j}(\tau)$ for each fluid node given by Eq. (9):

$$T_{f,j}(\tau) = (f * g_j)(\tau) + T_{0,j}(\tau) = (f * g_j)(\tau) + (f_0 * g_{0,j})(\tau) \quad (9)$$

where $T_{0,j}(\tau)=(f_0*g_{0,j})(\tau)$, contrary to T_0 in Eq. (8), is not necessarily constant in-depth and can vary in time. The present study highlights also that the effect on the TRT analyses due to the q_{ratio} parameter is directly correlated to the dimensionless g_0-transfer function evaluated from the numerical solution $S_j(\tau)$ by performing a complete circulation test of the same duration of the TRT without conferring any heat input rate. Eq.(9) denotes that the general solution $T_{f,j}(\tau)$ for each fluid node is given by superposing in time two different solutions (two different/separated convolutions). The k_{gr} that has to be estimated in the TRT is hidden inside both the $g_j(\tau)$ and $g_{0,j}(\tau)$ transfer functions. The external heat input rate is incorporated into the external excitation function $f(\tau)$ and expressed in terms of the fluid temperature difference imposed by the TRT machine at the BHE inlet and outlet sections. The excitation $f_0(\tau)$ is needed only in presence of non-zero $dT_{gr,\infty}/dz$. Both $f(\tau)$ and $f_0(\tau)$ have to be convolved with each $g_j(\tau)$ and $g_{0,j}(\tau)$ dimensionless functions respectively (for each j_{th} node, for any time τ). The $g_j(\tau)$ and $g_{0,j}(\tau)$ functions related to each j_{th} node of fluid volume are evaluated from the simulated (or experimental) temperature profiles $S_j(\tau)$ resulting from the complete numerical model (the three FD Models considered in the present study). The $g_{0,j}(\tau)$ functions take into account the effect related to the undisturbed ground temperature profile which is particularly important in the case of a non-zero geothermal gradient in the TRT analysis. The $g_{0,j}(\tau)$ functions are derived by simulating the TRT (or performing the real test) with no thermal inputs. This incorporates the effect on TRT of any specific non-uniform temperature distribution. When q_{ratio} is lower than 1, the effect of the geothermal gradient incorporated into the $g_{0,j}(\tau)$ function, is able to modify the slope of the general solution $T_{f,j}(\tau)$ for each fluid node, as graphically shown by Figure 1 (expressed in terms of $T_{f,ave}(\tau)$, see Appendix A). The $T_{f,ave}(\tau)$ profiles computed by the FD Model and reconstructed by the $T_{f,j}(\tau)$ profiles from Eq. (9) are reported as an example in Figure 1. The simulated case has been performed according to the input data related to the 800 m cases reported in [8] and collected in Table 1; in particular, the one denoted with "Case 800/40" related to the center inlet configuration of the coaxial BHE. For the sake of completeness, it has to be reminded that when referring to 800/40, 800/-40, 800/213.33, 800/-213.33 for identifying each case, according to the nomenclature adopted by [8], the first number is the depth in meters and the second number is the related heat transfer rate per unit length, in W/m.

Table 1
Parameters used in simulations with the numerical model related to the 800 m coaxial, single and double U pipe DBHE (base case).

Parameter	*Coaxial 800 m*	*U pipe 800 m*
Borehole length	800 m	800 m
Borehole diameter	0.14 m	0.14 m
Pipe inner radius	0.045 m	0.0163 m

Pipe wall thickness	0.008 m	0.0037 m
Annular pipe inner radius	0.0695 m	-
Annular pipe wall thickness	0.0004 m	-
Shank spacing	-	0.06 m
Mass flow rate	2.55 kg/s	2.55 kg/s
Fluid thermal conductivity	0.60 W/(m·K)	0.60 W/(m·K)
Fluid density	1000 kg/m^3	1000 kg/m^3
Fluid specific heat capacity	4186 J/(kg·K)	4186 J/(kg·K)
Fluid dynamic viscosity	1.0 x 10^{-3} kg/(m·s)	1.0 x 10^{-3} kg/(m·s)
Pipe thermal conductivity	0.42 W/(m·K)	0.42 W/(m·K)
Grout thermal conductivity	-	1.2 W/(m·K)
Grout volumetric heat capacity	-	1.35 MJ/(m^3·K)
Local borehole thermal resistance (coaxial)	0.00378 (m·K)/W	-
Ground surface temperature (z = 0)	281.15 K	281.15 K
Heat injection/extraction rate	32 kW (Case 800/±40); 170 kW (Case 800/±213.33)	
Duration of fluid circulation prior to heat injection/extraction	4 h	4 h
Duration of heat injection/extraction	90 h	90 h

As illustrated in Figure 1, the ILS-based k_{gr} estimation when the $g_{0,j}(\tau)$ function is taken into account differs by -14.3 % from the ILS-based k_{gr} estimation without taking into account the effect related to the geothermal gradient incorporated into the $g_{0,j}(\tau)$ function (the reference value for k_{gr} used in the FD model is 3 W/mK). The correct estimated k_{gr} value from the ILS-based TRT analysis can be obtained only by removing the $g_{0,j}(\tau)$ function from the real (in this case simulated) TRT data.

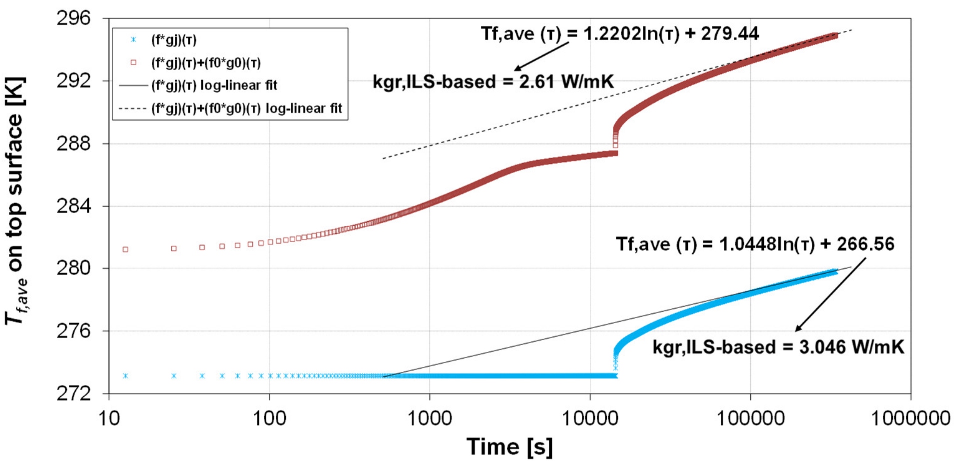

Figure 1: Fluid temperature profiles computed by FD Model as reconstructed by the $T_{f,j}(\tau)$ profiles from Eq. (9) (in terms of $T_{f,ave}(\tau)$ on top surface, geothermal gradient set to 0.02 K/m, q_{ratio} <1) related to the Center inlet case of Case 800/40.

Figure 1 shows how the evaluation and removal of the g_0 function from any TRT data would be of great importance to remove the geothermal gradient influence (highlighted by q_{ratio} <1) and obtain the correct k_{gr} estimations from any TRT analysis based on the ILS model (for single and, as it will be shown in section 4, also for multiple ground layers).

The $T_{0,j}(\tau)=(f_0*g_{0,j})(\tau)$ functions related to the single and double U-pipes have been compared with those related to the coaxial BHEs (center-inlet and annular-inlet hydraulic configurations) in the case of the geothermal gradient is 0.02 K/m, as reported in Figure 2. These simulated cases reported as an example have been performed according to the input data of the 800 m cases reported in [8] and collected in Table 1. Since 94 hours of circulation without any heat input rate are needed to compute the $T_{0,j}(\tau)=(f_0*g_{0,j})(\tau)$ functions, the profiles reported in Figure 2 for the inlet and outlet nodes necessarily overlap for each same BHE-configuration type.

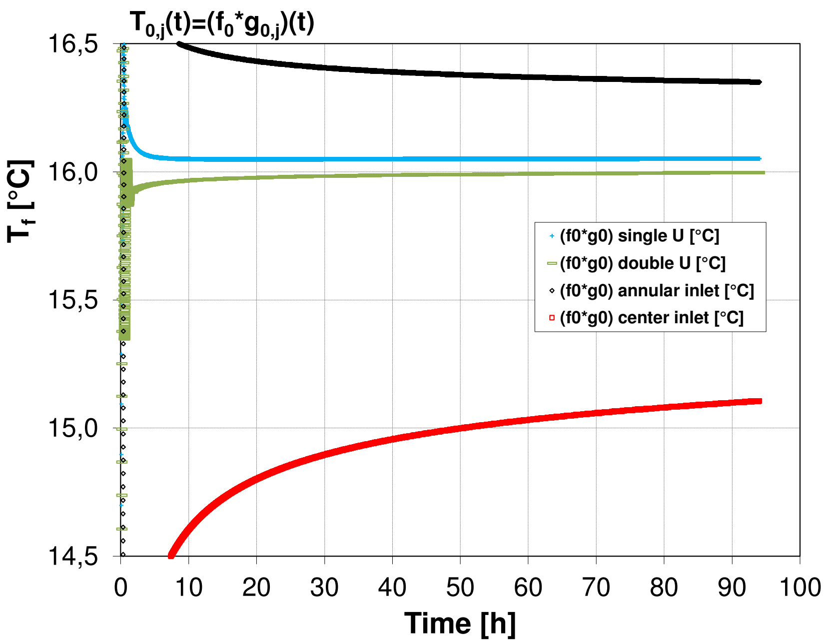

Figure 2: The comparison between the $T_{0,j}(\tau) =(f_0*g_{0,j})(\tau)$ functions related to the 800 m coaxial, single and double U-pipes (geothermal gradient set to 0.02 K/m).

The results reported in Figure 2 clearly show that the $T_{0,j}(\tau)$ profile related to the center inlet configuration of the coaxial case changes much more at late times than the $T_{0,j}(\tau)$ profiles related to the annular inlet, single and double U pipe (for the same borehole length of 800 m). While the $T_{0,j}(\tau)$ functions related to the inlet and outlet nodes assume a value close to being a constant for the single and double U pipes for almost the entire duration of a TRT, it can be noticed how the $T_{0,j}(\tau)$ functions related to the inlet and outlet nodes assume a slight slope in the case of the coaxial center inlet case. According to [8] and contrary to what the ILS model assumes, for a DBHE in presence of a non-zero geothermal gradient, the thermal equilibrium temperature $T_{gr,\infty}$ between the fluid and the surrounding ground reached at the end of the circulation period does not correspond to the mean value along the BHE active depth H of the undisturbed ground temperature, especially for the coaxial center-inlet case. This is symptomatic of the almost nil contribution of additional heat input rate related to the available geothermal heat flux within the BHE length H in the case of the single and double U pipes, while a positive natural extra heat contribution in the case of the center inlet case. This confirms also that the $T_{0,j}(\tau)$ functions incorporate the contribution of an additional heat input rate related to the available geothermal heat flux within the BHE length H, then influencing the slope of the resulting $T_{f,j}(\tau)$ fluid profiles if not corrected through the proper choice of the best external heat transfer rate $\dot{Q}$ during the TRT. The $g_{0,j}(\tau)$ functions have an effect during the entire TRT duration (also during the heat input phase). In the case of q_{ratio} lower than 1 the $g_{0,j}(\tau)$ functions can modify the slope of the fluid temperature profiles, especially for the coaxial BHE. Also the Annular inlet case in Figure 2 shows a slight slope having a lower magnitude than the one of the center inlet case for the overall duration of the TRT. This represents another perspective that allows understanding why in the case of q_{ratio} <1, the annular inlet configuration confers better ILS-based k_{gr} estimation than the center inlet one (for both heat injection and heat extraction scenarios) as reported in [8].

The smaller changes of $T_{0,j}(\tau)$ with time in Fig. 2 for the U-pipe configuration can be explained as follows. Picture a stationary elemental fluid volume of thickness dz in one of the U-pipes. If the flow is downward through the pipe, the geothermal gradient tends to cause cooler fluid from above to enter the elemental volume. On the other hand, for upward flow in the other side of the U-pipe, the geothermal gradient tends to make warmer fluid enter the elemental volume from below. The effects on the fluid in each pipe are likely to have similar magnitudes but oppose each other (source/sink). They are more likely to cancel each other. In the coaxial BHE, the fluid in the annulus has a more direct pathway to heat exchange with the ground than the fluid in the center pipe. In order for the fluid in the center pipe to gain or lose heat with the ground, the heat must travel through the annular fluid. Thus, the heat transfer is indirect between the ground and the center-pipe fluid. Without the symmetry of the U-pipe arrangement, the effects are unbalanced on the two flow streams. Thus, the opposing effects (source/sink) are more likely to have different magnitudes and do not cancel. This unbalance makes the net effect larger in the coaxial borehole.

According to Pasquier and Marcotte [39,40] the convolution products $(f*g_j)(\tau)$ and $(f_0*g_{0,j})(\tau)$ in Eq. (9) are computed in the frequency domain using the spectrum of f and g_j (f_0 and $g_{0,j}$); this is much faster than the standard convolution in the time domain. According to Eq. (7), the expressions $(f*g_j)(\tau)$ and $(f_0*g_{0,j})(\tau)$ in Eq. (9) are computed through Eqs. (10) and (11):

$$\left(f * g_j\right)(\tau) = F^{-1}\left(F(f) \cdot F(g_j)\right) \tag{10}$$

$$\left(f_0 * g_{0,j}\right)(\tau) = F^{-1}\left(F(f_0) \cdot F(g_{0,j})\right) \tag{11}$$

For more details on the *FFT* method, the Reader is addressed to read [40,41]. The present approach exploiting the specific strengths of the *FFT* method in handling different types of boundary conditions (i.e. variable heat input rate above the ground and an undisturbed ground temperature profile which can be uniform or variable along the depth) saves a lot of the computation CPU time to run each simulation (provided that f, f_0, g_j and $g_{0,j}$ have been obtained). This is because any change of the external heat input rate involves only the external excitation function $f(\tau)$ that is convolved with each evaluated and invariant dimensionless $g_{,j}(\tau)$ function and superposed with the $(f_0*g_{0,j})(\tau)$ convolution product (for each node, for any time). On the other hand, the $g_{0,j}(\tau)$ functions are derived by simulating the model (or performing the real test) with no thermal inputs to properly take into account the effect related to the undisturbed ground temperature profile which is particularly important in the case of a non-zero geothermal gradient. The *FFT* method adopted in this work for computing the convolution products incorporates concepts based on the studies by [39,40,41,50].

2.1 Methodology

Three Fortran90 programs implementing the FD Models related to coaxial, single and double U-BHE geometries presented in [4,20,21] are exploited to evaluate the $g_j(\tau)$ and $g_{0,j}(\tau)$ functions related to each j_{th} node of fluid volume. These models have been proved and validated against available literature TRT measurements, showing very accurate thermal profiles which overlap those related to the experimental data as reported in [4,20,21]. The Reader is directed to those papers for a complete model description. A dedicated Fortran90 program, whose results have been successfully cross-checked with those provided by an independent Matlab solver, implements the routine for performing the FFT computation used to reconstruct the $T_{f,j}(\tau)$ temperature profiles from the FD Models. The dedicated Fortran90 code allows the choice of subgroups of nodes for the reconstruction of the $T_{f,j}(\tau)$ for each j_{th}-node. The $g_{0,j}$-function in the term $(f_0*g_{0,j})(\tau)$ is the only term on the right-hand side of Eq. (9) with information about the geothermal gradient. The g_j-function in the term $(f*g_j)(\tau)$ is evaluated by ignoring the geothermal gradient. The evaluation of the g_j-function in the term $(f*g_j)(\tau)$ uses a uniform undisturbed ground temperature (constant with depth) profile whose value is imposed everywhere equal to 0 °C= 273.15 K (assumption proper of the method to evaluate the g_j for each node). To evaluate the values related to g_j for each fluid node, it is needed to run an entire numerical simulation with one of the three complete FD Models considered in the present study, with a 0 °C assigned to all the nodes. This is obtained by imposing a zero-geothermal gradient in the fluid and ground domain as the initial condition and applying the desired value of the external heat input rate (it is possible to adopt whatever value of external heat input rate to evaluate the g_j function for each node because the boundary condition related to the external heat transfer rate is in any case handled by the $f(\tau)$ function). According to what is described in Pasquier and Marcotte [40,41] the dimensionless g_j functions are derived using the Eq.(12) reported hereafter:

$$g_j(\tau) = \frac{S_j(\tau)}{\beta} \tag{12}$$

The $S_j(\tau)$ term in the numerator is the solution computed by the complete FD numerical Model related to each node in the time domain ($S_j(\tau)$ in general can also represent the experimental temperature profile in a real test; in this last case, the $S_j(\tau)$ would already incorporate also the geothermal gradient effect, thus the $g_{0,j}(\tau)$ function) suitably converted in °C, according to the method described by Pasquier and Marcotte [41], while β is the constant for which $g_j(\tau= \tau_{start\ heat\ input\ rate})=1$, then:

$$\beta = \frac{\dot{Q}_{start\ heat\ input\ rate}}{\dot{m}c_f} \quad [°C] \tag{13}$$

The value related to the constant β depends on the choice of the $\dot{Q}_{start\ heat\ input\ rate}$ value; therefore the choice of the value of external heat transfer to evaluate the g_j-functions can be arbitrary since the solution $S_j(\tau)$ is in any case affected by this choice and made dimensionless by dividing by the constant β.
The $f(\tau)$ excitation function incorporates the effect related to the external heat input rate in terms of the temperature difference between the BHE inlet and outlet sections, in particular:

$$f(\tau) = \frac{\dot{Q}(\tau)-\dot{Q}(\tau_{i-1})}{\dot{m}c_f} \qquad [°C] \tag{14}$$

In a standard TRT, since the external load $\dot{Q}$ should be typically kept constant (around 90-100 hours of heat injection at constant power) the $f(\tau)$ assumes the values (for each time step included in the defined τ window):

$$f(\tau) = [\frac{\dot{Q}_{start\ heat\ input\ rate}}{\dot{m}c_f}, 0, 0, 0, 0, \ldots, 0] \quad \forall\ \tau_{start\ heat\ input\ rate} \le \tau \le \tau_{end\ experiment} \tag{15}$$

To evaluate the values related to $g_{0,j}$ for each fluid node, in the present study the entire 94-h TRT simulated with the complete FD Model for coaxial BHE has been run taking into account the geothermal gradient thus the actual values of the undisturbed ground temperature profile imposed in the whole domain as the initial condition without considering any external heat input rate for all the entire duration of the experiment.
According to what is described in Nguyen et al. [50] the dimensionless $g_{0,j}$ functions are derived using the Eq.(16) reported hereafter:

$$g_{0,j}(\tau) = \frac{S_{0,j}(\tau)}{\beta = 1°C} \tag{16}$$

$S_{0,j}(\tau)$ is the solution in the time domain computed by the complete FD Model without taking into account any external heat input rate for the entire duration of the experiment. $S_{0,j}(\tau)$ is related to each node ($S_{0,j}(\tau)$ can also represent the experimental temperature profiles in a real test of complete circulation) suitably converted in °C, while β is the constant that makes $g_{0,j}(\tau)$ dimensionless but numerically equivalent to the $S_{0,j}(\tau)$ solution, then β = 1 °C.
The $f_0(\tau)$ excitation function assumes the values reported in Eq.(17) so that the convolution product $T_{0,j}(\tau) = (f_0 * g_{0,j})(\tau)$ coincides with the numerical solution $S_{0,j}(\tau)$ conferred by the FD Model (for each time step included in the defined τ window):

$$f_0(\tau) = [1, 0, 0, 0, 0, \ldots] \quad \forall\ 0 \le \tau \le \tau_{end\ experiment} \tag{17}$$

2.2 Validation of the method

As the validation of the FFT spectral method implemented in the dedicated Fortran90 program, it has been verified that the $T_{f,j}(\tau)$ solution provided by Eq. (9) coincides with the complete solution given by the FD Model run for the entire 94h simulated TRT related to the “Case 800/40” (non-zero geothermal gradient characterizing the undisturbed ground temperature profile imposed in the whole domain as the initial condition and conferring the proper external heat input rate starting from the 4th hour of the experiment). The fluid temperature profiles related to the coaxial center-inlet case simulated by the FD Model and reconstructed by the FFT method have been reported in Figure 3. During the pre-circulation phase of 4 hours without any external heat input rate (and the geothermal effect during circulation) only the $(f_0*g_{0,j})(\tau)$ term in Eq. (9) provides a numerical contribution (the contribution related to the convolution product $(f*g_j)(\tau)$ is zero when the external heat input rate is 0 W). When the external heat input rate starts both the terms in Eq. (9) provide a numerical contribution. Under these assumptions, Eq. (9) produces the temperature profile reported in Figure 3 related to the inlet node of the 800 m coaxial center-inlet case whose input data are reported in [8] and collected in Table 1. In this case, q_{ratio} is lower than 1 and the geothermal gradient is 0.02 K/m.

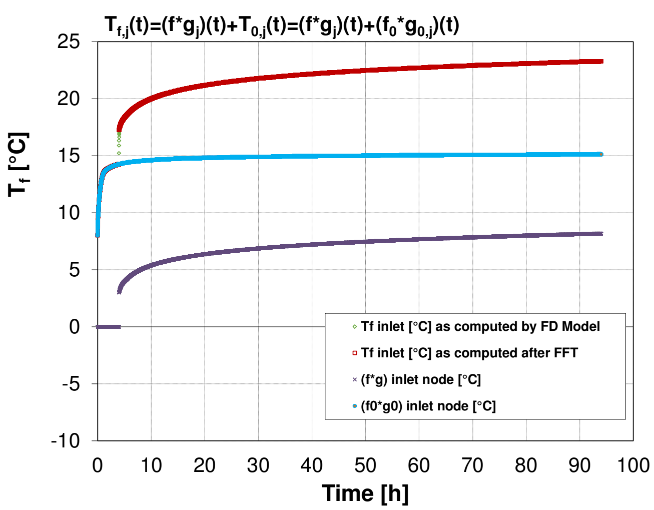

Figure 3: Fluid temperature computed by the FD Model as reconstructed by the superposition of the $(f*g_j)(\tau)$ and the $(f_0*g_{0,j})(\tau)$ profiles (for the inlet node, geothermal gradient set to 0.02 K/m, q_{ratio} <1) related to the Center inlet Coaxial DBHE of Case 800/40.

From Figure 3 inspection, it is straightforward to notice that the profile related to the inlet node computed by the FD Model overlaps with the one obtained from Eq. (9) during the whole test of 94h.

3. Application of the method for TRT analysis in the case of single-layer subsurface for coaxial, single and double U BHEs

The numerical results plotted in the Figures of the present section are aimed to explain how the present method related to the *FFT* technique is applied to reconstruct the fluid temperature profiles computed by the complete FD Models. For the sake of clarity, only the temperatures resulting from the application of the *FFT* method have been reported in the Figures of the present section since are the same as the FD model. Furthermore, the profiles related to the convolution product $(f*g_j)(\tau)$ have been reported in the Figures of the present section (while the $T_{0,j}(\tau)$ profiles are those reported in Figure 2 of the present paper). The results reported in the present section also graphically explain how the $g_{0,j}(\tau)$ function can influence the ground thermal conductivity estimation when the ILS model is employed in the TRT analysis. This is shown through simulations related to coaxial deep BHE of 800 m in presence of a single-layer subsurface with a non-zero geothermal gradient compared to the same case with an undisturbed ground temperature profile perfectly uniform along the depth.

According to Eq. (9), adding the convolution product $(f*g_j)(\tau)$ to the $T_{0,j}(\tau)$ profiles (those related to the Case 800/40 reported in Figure 2 of the present paper) produces the fluid temperature profiles shown in Figure 4. These temperature profiles are related to the inlet node of the 800 m coaxial (annular inlet and center inlet) and U-pipes (single and double U) BHEs in the case q_{ratio} is lower than 1, the geothermal gradient is 0.02 K/m, and a single layer subsurface having ground thermal conductivity value of 3 W/mK. The input data details related to these simulated cases are reported in Table 1, those denoted with "Case 800/40". For these cases, the external heat input rate per unit length is 40 W/m competing against the available natural geothermal heat rate of 48 W/m along the BHE depth (q_{ratio} lower than 1).

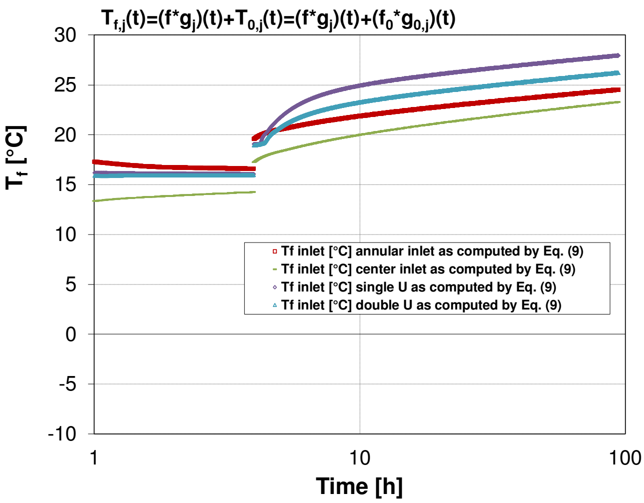

Figure 4: Fluid temperature from the superposition of the $(f*g_j)(\tau)$ and the $(f_0*g_{0,j})(\tau)$ profiles (for the inlet node, geothermal gradient set to 0.02 K/m, q_{ratio} <1) related to the coaxial and U - pipes of "Case 800/40".

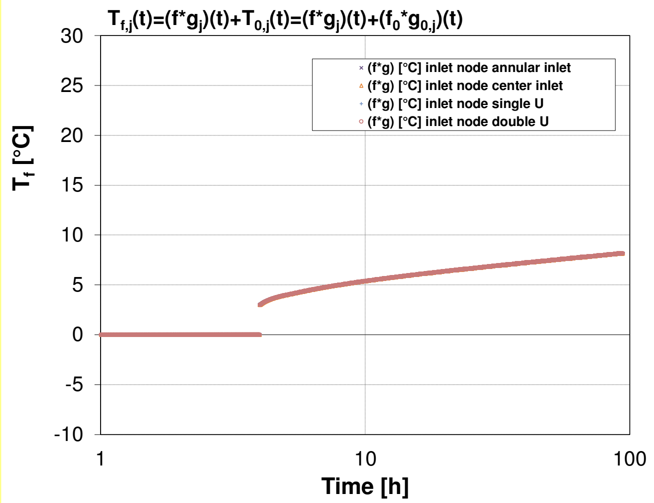

Figure 5: $(f{*}g_j)(\tau)$ profiles (for the inlet node) related to the coaxial and U - pipes of "Case 800/40".

The $(f{*}g_j)(\tau)$ profiles related to the Case 800/40 have been reported in Figure 5. As it is easy to notice, the $(f{*}g_j)(\tau)$ profiles reported in Figure 5 are almost overlapped for all the BHE types and hydraulic configurations. This is because the g_j-function in the term $(f{*}g_j)(\tau)$ is evaluated by ignoring the geothermal gradient and a value equal to 0 °C= 273.15 K (constant with depth) is imposed in the fluid and ground domain as the initial condition. Figure 4 together with Figure 5 are aimed to show the effect due to the $g_{0,j}(\tau)$ functions (that is the geothermal gradient effect) embedded into the $T_{0,j}(\tau)$ functions related to each BHE type and hydraulic configuration. In particular, Figure 4 confirms what is highlighted by Figure 2 on how the $T_{0,j}(\tau)$ functions and the $T_{gr,\infty}$ value reached at the end of the pre-circulation phase of 4 hours, prior to the start of heat injection (or extraction) of a TRT, do not coincide among the coaxial and U-pipes cases when the geothermal gradient is 0.02 K/m. If the geothermal gradient would have been perfectly 0.0 K/m all the fluid temperature profiles shown in Figure 4 would almost coincide as they would differ from those shown in Figure 5 for a constant equal to T_0 that is the uniform ground temperature profile over the domain's height (zero geothermal gradient). The present investigation at q_{ratio} <1 (whose resulting profiles are shown in Figure 4) graphically confirms that, as opposed to both coaxial cases, the U-pipes are less influenced by the absolute value of q_{ratio} when the ILS model is used for the ground thermal conductivity estimation from TRT data. This is graphically shown by the almost equal slopes characterizing the late time of the test for the U-pipes and the different slopes assumed by the coaxial arrangements in Figure 4. As well as the $T_{gr,\infty}$ value reached at the end of the pre-circulation phase of 4 hours is almost equal for the U-pipes while differs between the coaxial configurations (as confirmed by [8]). The $T_{0,j}(\tau)$ functions and in particular the $g_{0,j}(\tau)$ functions incorporate the main numerical reason for which the coaxial cases are more sensitive to the q_{ratio} parameter (to the geothermal gradient effect) than the U-pipes when the ILS model is used to estimate the ground thermal conductivity, as confirmed by the ILS-based k_{gr} estimation results reported in [8] and collected in Table 2. The FOA-ILS-based analysis has been made for different Fo_{rb} intervals in the range $10 \leq Fo_{rb} \leq 66.12$ by varying the starting Fo_{rb} from 10 to 55 in increments of 5. For the sake of brevity, the k_{gr} FOA-ILS-based estimated values from Eq. (A.9) in the range $10 \leq Fo_{rb} \leq 66.12$ have been reported in Table 2. The definition of Fo_{rb} is given in Eq. (A.4). The reader is addressed to [8] for a complete and detailed description of the ILS-based analysis and related results briefly reported in the present section.

Table 2

Ground thermal conductivity estimated values considering the $10 \leq Fo_{rb} \leq 66.12$ interval compared to the k_{gr} value (3.0 W/(mK)) imposed in the single layer subsurface, geothermal gradient set to 0.02 K/m.

Case	k_{gr} (ILS-estimated value)	|% Error|
800/40 Center inlet	2.593 [W/mK]	13.55 %
800/40 Annular inlet	3.177 [W/mK]	5.90 %
800/40 single U	2.905 [W/mK]	3.16 %
800/40 double U	2.917 [W/mK]	2.77 %
800/213.33 Center inlet	2.937 [W/mK]	2.10 %
800/213.33 Annular inlet	3.058 [W/mK]	1.94 %
800/213.33 single U	2.904 [W/mK]	3.20 %
800/213.33 double U	2.941 [W/mK]	1.96 %

The same numerical simulations have been performed in the case of a geothermal gradient of 0.0 K/m. For the sake of brevity, only the fluid temperature profiles related to coaxial cases have been presented and reported in Figure 6. In these cases, the $T_{gr,\infty}$ value reached at the end of the circulation phase corresponding to the previous simulations reported in Figure 4 for each coaxial case (annular inlet and center inlet) is directly imposed uniformly along the ground depth from the beginning of the test. As previously, these temperature profiles are related to the inlet node of the 800 m coaxial (annular inlet and center inlet). The profiles related to the convolution product $(f{*}g_j)(\tau)$ are the same reported in Figure 5 (in this case the $T_{0,j}(\tau)$ profiles are not plotted since they are related to a geothermal gradient of 0.0 K/m, thus invariant in time and equal to the $T_{gr,\infty}$ constant value corresponding to the uniform in-depth initial condition).

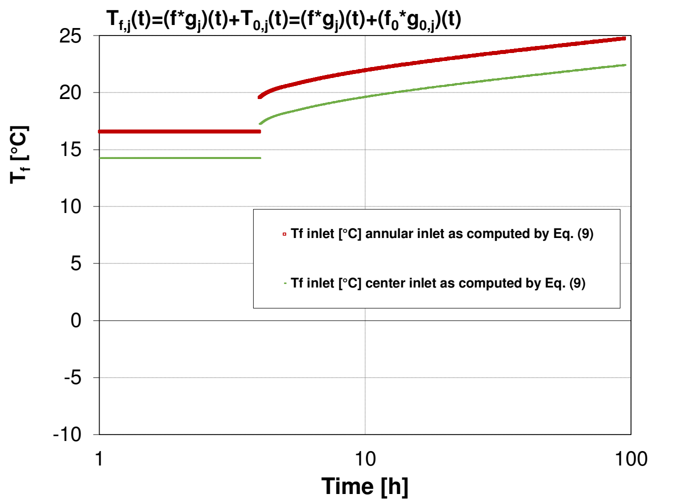

Figure 6: Fluid temperature from the superposition of the $(f*g_j)(\tau)$ and the $(f_0*g_{0,j})(\tau)$ profiles (for the inlet node, geothermal gradient set to 0.0 K/m) related to the coaxial DBHE of "Case 800/40".

Since the geothermal gradient is 0.0 K/m all the fluid temperature profiles shown in Figure 6 differ from those shown in Figure 5 for a constant equal to T_0 which is the uniform ground temperature profile over the domain's height (zero geothermal gradient), a different constant between the coaxial cases. In this case, the $g_{0,j}(\tau)$ functions related to the inlet and outlet nodes do not influence the slope of the resulting $T_{f,j}(\tau)$ fluid profiles (nil contribution of additional heat input rate related to the available geothermal heat flux within the BHE length H since the geothermal gradient of 0.0 K/m). Therefore the corresponding ground thermal conductivity estimation from the ILS model will result very close to each other (regardless of the choice of the hydraulic configuration). This is also observed by similar fluid temperature profiles obtained from simulated TRTs with a zero geothermal gradient reported in [20] and the related k_{gr} ILS-based estimations.

According to the "800/213.33" coaxial case reported in [8] and presented in Table 1, Figure 7 graphically shows how in presence of the geothermal gradient of 0.02 K/m and q_{ratio} >>1, the fluid temperature profiles can assume the slope (in the semi-logarithmic time scale) compatible with the ground thermal conductivity value of 3 W/mK imposed in the program input file also in case the center inlet configuration is adopted (see Table 2). This case for which q_{ratio} is greater than 1 has been reconstructed by the FFT according to the present method synthetically represented by Eqs. (9), (10) and (11). The fluid temperature profiles related to q_{ratio} >>1 for the inlet node have been reported and compared with those related to q_{ratio} < 1 in Figure 7.

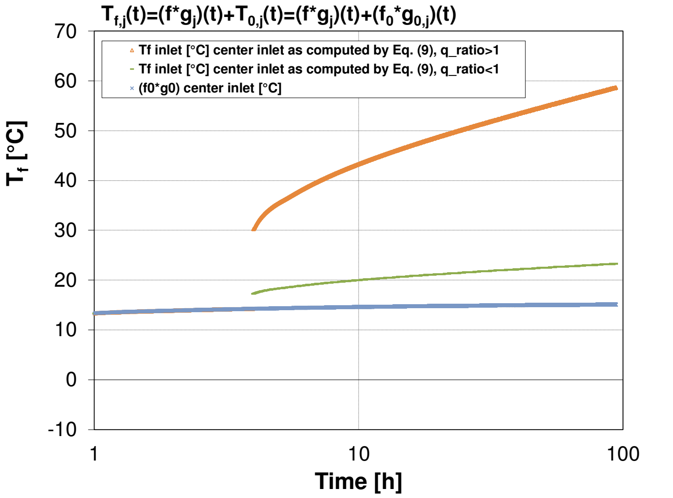

Figure 7: Fluid temperature from the superposition of the $(f^*g_j)(\tau)$ and the $(f_0{}^*g_{0,j})(\tau)$ profiles (for the inlet node, geothermal gradient set to 0.02 K/m, q_{ratio} >>1) compared with those obtained for q_{ratio} <1 related to the Center inlet case of Case 800/213.33.

From Figure 7 inspection, it is straightforward to notice how in the case of q_{ratio} >>1 the contribution of heat input rate related to the $T_{0,j}(\tau)$ function is too lower compared to the one provided by the external heat input rate imposed (external heat input rate per unit length of 213.33 W/m against the available natural geothermal heat rate of 48 W/m along the BHE depth). In this case, the effect of the external heat input rate on the fluid temperature profiles greatly overrides the relatively small contribution related to the natural geothermal one. For the single-layer subsurface case, the condition related to q_{ratio} >>1 guarantees the correct ground thermal conductivity estimation for both the hydraulic configurations when the ILS model is used in TRT analysis, as confirmed by the ILS-based k_{gr} estimation results reported in Table 2.

4. Application of the method for TRT analysis in the case of multiple ground layers of equal thickness with geothermal gradient

A series of simulations has been carried out to investigate if the q_{ratio} is the dominant parameter when the ILS model is used to estimate the ground thermal conductivity, also in presence of different ground layers of equal thickness with different thermal conductivity values imposed along the depth. In particular, the numerical simulations reported in the present section aimed to demonstrate the influence of q_{ratio} along with the impact of other dimensionless parameters specific to TRTs. The results for ground with multiple layers are of particular interest because no previous research systematically studies these effects. The investigation reported in the present section is mainly focused on the coaxial case, which is the most likely configuration for deep boreholes and, as shown in the previous sections, the most affected by the effects due to q_{ratio}. Any changes in the r_b/H and $\dot{m}/H$ ratios are not able to mitigate the influence related to the q_{ratio} parameter on the ground thermal conductivity estimation when the ILS model is employed. The results reported in the present section have been graphically explained and clarified also in terms of $g_{0,j}(\tau)$ functions. The analysis considers different ground layers of equal thickness with different thermal conductivity values imposed along the depth and corresponding geothermal gradients. The condition related to q_{ratio} >>1 has to be satisfied in an ILS-based TRT analysis in order to override the additional heat input rate (particularly prominent for coaxial DBHEs) provided and incorporated into the $g_{0,j}(\tau)$ functions. The q_{ratio} >>1 condition guarantees the ILS-based k_{gr} estimation moving closer to the mean k_{gr} value among the layers.

The main input parameters are reported in Table 1 according to those reported in Beier et al. [24] while the grid properties characterizing the numerical simulations related to the 800 m coaxial DBHE case are reported in Table 3. The k_{gr} values and geothermal gradients for each layer follow the list in Table 4, also reported in [24]. According to Eq. (2.2), the ground thermal conductivity k_{gr} increases with depth as listed in Table 4 while the geothermal gradient $dT_{gr,\infty}/dz$ decreases as their product remains constant in each layer and equal to 0.04 W/m^2. For layered ground, the (0.04 W/m^2) value of the density of natural heat flux has been adopted in each layer according to [24]. The k_{gr} values of the ground surrounding the simulated borehole are not specific to the geology related to any location but generically represent a range of possible physical values. In the DTRT simulations reported in the present study, the ground is made of four layers, each having a different k_{gr} value. The heat extraction rate per meter from the ground is kept at 40 W/m. The case 800/(-40) is named "CASE 3A" in the present section and, according to [24], can serve as a base case because the heat extraction rate (W/m) is in the typical range.

Table 3
Grid properties characterizing the numerical simulations related to the 800 m coaxial DBHE (base case).

Input type	Value
Domain end radial *r*-coordinate	3.2 m
Domain end axial *z*-coordinate	840 m
Number of partitions along the *r*-direction	30
Number of partitions along the *z*-direction	80
Finite increment Δz	10.5 m
Time step $\Delta\tau$	10.51 s

Table 4
Thickness, ground thermal properties and geothermal gradient of ground layers.

Layer	***Depth interval (m)***	$k_{gr,p}$ ***(W/(m·K))***	$\alpha_{gr,p}$ ***(m²/s)***	$(\rho c)_{gr,p}$ ***(J/m³K)***	***Geothermal gradient (K/m)***
1	0 to 200	1	3.33 x 10^{-7}	3.0 x 10^6	0.04
2	201 to 400	1.7	5.66 x 10^{-7}	3.0 x 10^6	0.0235
3	401 to 600	2.4	8.0 x 10^{-7}	3.0 x 10^6	0.0167

4	601 to 800	3.1	1.03×10^{-6}	3.0×10^{6}	0.0129

A series of simulations for the coaxial pipe adopting the same main input data related to the 800 m base case (named "CASE 3A") has been performed by varying the borehole depth (100 m to 800 m, "CASE 3B" to "CASE 3A BIS") while keeping the thickness of each layer equal to ¼ of the total depth. The TRT simulations for both the hydraulic configurations of the coaxial BHE have been performed for each case. The main input and pre-processing data which distinguish and identify each case are summarized in Table 5. Note as the depth decreases the magnitude of q_{ratio} increases since the heat extraction rate per meter is kept at 40 W/m. It has to be specified that the values related to the natural heat rate per unit length reported in Table 5 have been computed according to Eq. (2.1) where the ground thermal conductivity is the arithmetic average value among the layers, in this case, equal to 2.05 [W/mK]. The product between the ground thermal conductivity k_{gr} and the geothermal gradient $dT_{gr,\infty}/dz$ is constant for each layer (this product was chosen equal to 0.04 W/m^2) and used in Eq. (2.1). For layered ground, the average is the effective ground thermal conductivity for parallel heat conduction through layers with boundary conditions of uniform temperature at each end. In the case of layers with equal thickness, the average is the simple mean.

Table 5

Main input and pre-processing data identifying the center inlet and annular inlet cases.

Case	*$\dot{m}$ [kg/s]*	*$\dot{m}/H$ [kg/ms]*	*H [m]*	*External heat extraction rate $\dot{Q}$ [W]*	*Natural heat rate per unit length [W/m]*	*q_{ratio} [-]*
3B	0.32	0.0032	100	4,000	4	10
3C	0.64	0.0032	200	8,000	8	5
3D	0.95	0.0032	300	12,000	12	3.33
3E	1.27	0.0032	400	16,000	16	2.5
3F	1.59	0.0032	500	20,000	20	2
3G	1.91	0.0032	600	24,000	24	1.66
3H	2.23	0.0032	700	28,000	28	1.43
3A	2.55	0.0032	800	32,000	32	1.25

3A BIS	2.55	0.0032	800	170,667	32	6.66

The mass flow rate varies among the cases in order to keep the fluid temperature difference $(T_{in}\text{-}T_{out})$ constant at the top of the BHE, while $\frac{\dot{Q}}{H}$ remains constant (except for the CASE 3A BIS). This case has been purposely simulated and reported to show the corrective effect provided by the q_{ratio} >>1 on the ILS-based k_{gr} estimation in comparison to CASE 3A. The simulations and analyses reported in the present section for multiple ground layers indicate that the ILS-based k_{gr} estimation changes with q_{ratio}. Figure 8 shows the results for cases as the borehole depth decreases (800 m to 100 m), which increases q_{ratio}.

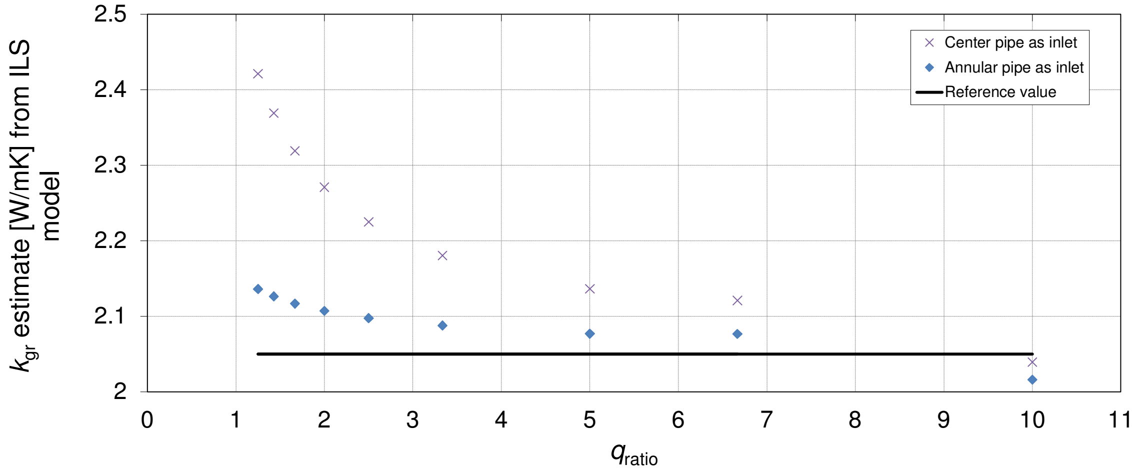

Figure 8: Effective ground thermal conductivity estimation from the FOA of the ILS model compared to the reference value (horizontal line).

Figure 8 compares the FOA-ILS-based k_{gr} estimation with the weighted-thickness average for the ground layers. In this case of layers with equal thickness, the average is the simple mean (the horizontal line is the reference value). The starting time of the time window for the ILS model is Fo_{rb}=10. The results indicate that as q_{ratio} decreases the ILS-based k_{gr} estimation departs from the arithmetic average. The same investigation has been carried out also considering different Fo_{rb} dimensionless time windows, producing the graph reported in Figure 9 (for the center inlet) and Figure 10 (for the annular inlet) configurations. The Fourier number Fo_{rb} corresponds to the starting time for the ILS model fit.

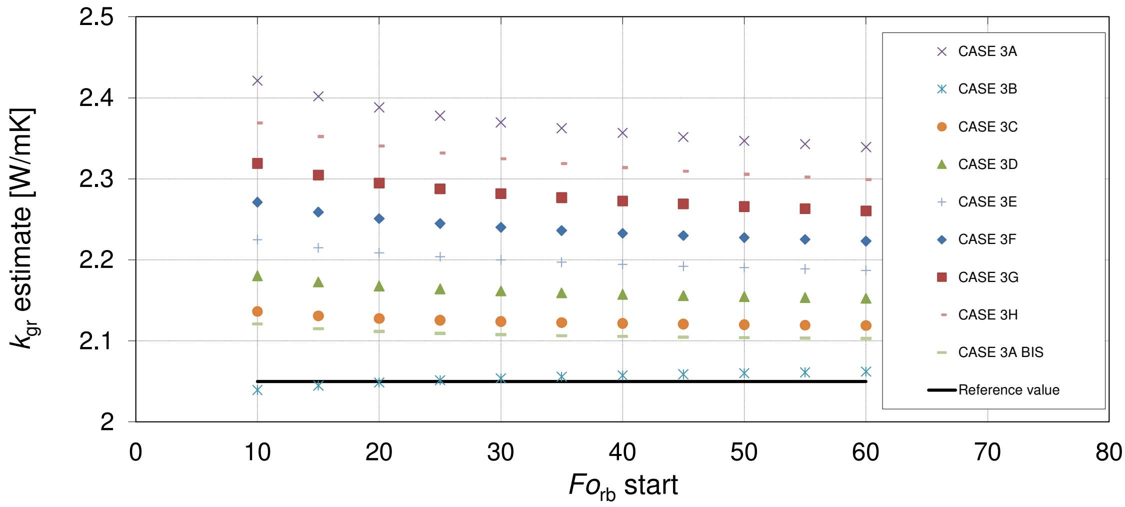

Figure 9: Effective ground thermal conductivity from the ILS model as estimated for different Fo_{rb} windows for the center inlet configuration.

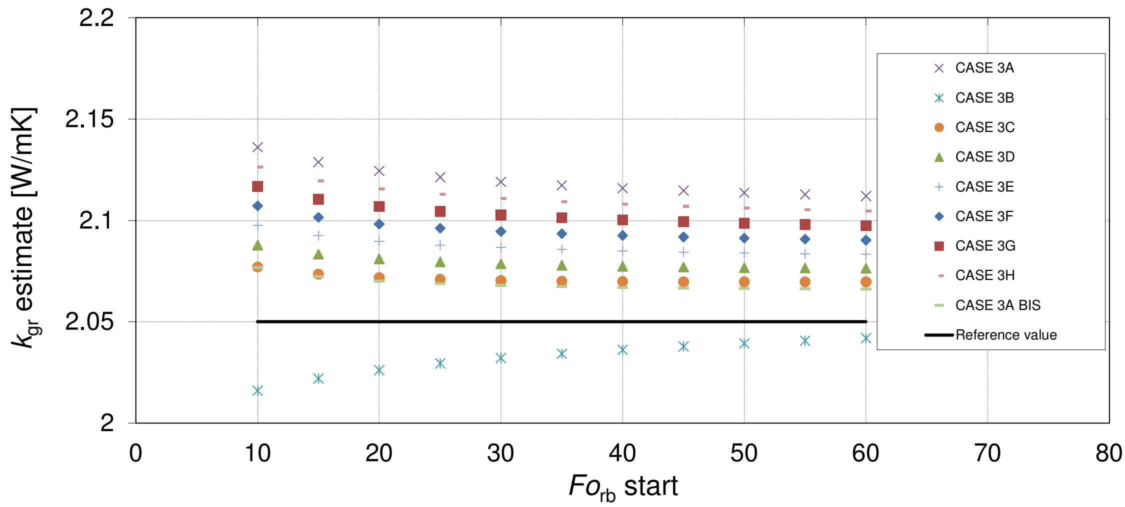

Figure 10: Effective ground thermal conductivity from the ILS model as estimated for different Fo_{rb} windows for the annular inlet configuration.

The analysis has been made for different Fo_{rb} intervals in the range $10 \leq Fo_{rb} \leq 66.12$ by varying the starting Fo_{rb} from 10 to 55 in increments of 5. The Fo_{rb} value of *66.12* at the end of the TRT remains fixed, which is related to the end of the 90-h period of heat extraction. The k_{gr} estimated values have been obtained for each Fo_{rb} window according to the FOA-ILS-based Eq. (A.9). From Figures 9 to 10 inspection, it is interesting to notice that, as one can expect, as the starting Fo_{rb} is varied becoming closer to the Fo_{rb} value of *66.12* at the end of the TRT, the k_{gr} estimations from the FOA-ILS-based Eq. (A.9) tend to move towards the mean k_{gr} value among the layers, especially for the cases characterized by a q_{ratio}

close to 1. This is because the effect related to the thermal transient characterizing the first hours of the TRT tends to weigh less when Fo_{rb} windows closer to the end of TRT are considered in the analysis.

As in the previous papers by the Authors [8,24], the ratio $\frac{\dot{m}}{H}$ has been kept constant among the cases by adjusting $\dot{m}$. The simulations demonstrate that when a strong geothermal gradient exists the difference between the FOA-ILS-based k_{gr} estimation and the mean k_{gr} tends to decrease as the total depth decreases. The parameter q_{ratio} is an indicator of this difference because as the total depth decreases, the q_{ratio} increases since the heat extraction rate per meter is kept at 40 W/m. The simulations demonstrate that as the depth decreases the estimated effective k_{gr} from the line-source model moves closer to the mean k_{gr}. This is due to the q_{ratio} parameter, as clearly demonstrated by the additional simulation (CASE 3A BIS) for the 800 m case with the heat extraction rate per meter from the ground set to 213.33 W/m. The additional simulation (CASE 3A BIS) demonstrates that the estimated effective k_{gr} from the ILS model moves closer to the mean k_{gr} when q_{ratio} >>1. This demonstrates once more how q_{ratio} is the most relevant among the parameters characterizing the TRT analyses, also in presence of multiple ground layers of equal thickness with different thermal conductivity values imposed along the depth. For the coaxial BHEs, the estimated k_{gr} from the ILS model moves closer to the mean k_{gr} value among the layers only if q_{ratio} >>1 regardless of the k_{gr} variations among the layers. The simulations demonstrate also that the movement in the line-source estimates of the effective k_{gr} from the mean is less for the annulus inlet configuration. The corresponding cases with the annulus as the inlet have significantly smaller deviations from the average k_{gr} (compare Fig. 10 to Fig. 9). The movement in the line-source estimates from the mean k_{gr} are expected to be in general less also for single and double U-tube configurations for ground with layers of equal thickness.

Other parameters related to the coaxial geometry have been varied with the dimensionless groups reported in Morchio et al. [8] exploiting the cluster of simulations reported in the present paper. The list includes the parameter N_1 related to the short-circuit thermal resistance, R_1, between each node placed in the center and annular pipe:

$$N_1 = \frac{H}{\dot{m}\, c_f\, R_1} \tag{18}$$

The N_2 and N_{gr} are the other dimensionless parameters in the list that include the $\frac{\dot{m}}{H}$ ratio:

$$N_2 = \frac{H}{\dot{m}\, c_f\, R_2} \tag{19}$$

$$N_{gr} = \frac{2\pi k_{gr} H}{\dot{m}\, c_f} \tag{20}$$

The parameter N_2 is related to the thermal resistance, R_2, between each node placed in the annular pipe and the borehole wall node. The parameter N_{gr} is the dimensionless conductance of ground, according to [8]. In the simulations whose results are reported in Figures 8, 9 and 10 of the present paper the $\frac{\dot{m}}{H}$ ratio is constant. The parameters N_1, N_2 and N_{gr} remain almost constant among the cases since containing $\frac{\dot{m}}{H}$ (slight variations are due to R_1 and R_2 variations among the cases because of the fluid velocity variation caused by different mass flow rate values). The study has been expanded by varying $\frac{\dot{m}}{H}$ with respect to the previous cases while keeping the q_{ratio} values constant and equal to those corresponding to the cases reported in Table 5 of the present paper. Cases in Beier [35] for uniform k_{gr} indicate changes of $\frac{\dot{m}}{H}$ has little influence on the estimate of k_{gr} from a 1D radial model until $\frac{\dot{m}}{H}$ becomes small. In the present paper, the effects of N_1, N_2 and N_{gr} have been studied by varying $\frac{\dot{m}}{H}$ for multi-layer ground. The other dimensionless parameters reported in [8] are area ratios and thermal property ratios, which would tend not to change for a given borehole under various TRT conditions.

Additional simulations for the same cases reported in Table 5 of the present paper have been performed adopting the half value of the $\frac{\dot{m}}{H}$ reported in Table 5 varying the mass flow rate among the cases in order to keep the $(T_{in}-T_{out})$ constant at the top of the BHE, while $\frac{\dot{Q}}{H}$ remains constant except for the CASE 3A BIS). For the sake of brevity, the graphs reporting the results of this simulations cluster have not been reported since the trends are not too dissimilar to those reported in Figures 8, 9, 10.

Another cluster of simulations has been performed at a third flow rate for each case in order to verify and consolidate if q_{ratio} is always the dominant parameter in the ILS estimation of the k_{gr} for more different $\frac{\dot{m}}{H}$ values (for both the center and annular inlet configuration of the coaxial cases). In particular, the mass flow rate related to the 200 m CASE 3C has been imposed on the 100 m and 300 m cases (3B and 3D respectively) while the cases from 400 m to 800 m (3E to 3A BIS respectively) adopt the mass flow rate related to the 600 m CASE 3G, as reported in Table 6. In this manner, 7 of the 9 cases are characterized by a different $\frac{\dot{m}}{H}$ value and the fluid temperature difference between the BHE inlet and outlet sections is kept included between 1.5°C and 4.5°C except for the CASE 3A BIS. The related results are reported in Figures 11, 12 and 13.

Table 6

Main input and pre-processing data related to the center inlet and annular inlet cases varying $\frac{\dot{m}}{H}$ among the cases.

Case	*$\dot{m}$ [kg/s]*	*$\dot{m}/H_b$ [kg/ms]*	*H_b [m]*	*External heat extraction rate $\dot{Q}$ [W]*	*Natural heat rate per unit length [W/m]*	*q_{ratio} [-]*
3B	0.64	0.0064	100	4,000	4	10
3C	0.64	0.0032	200	8,000	8	5
3D	0.64	0.0021	300	12,000	12	3.33
3E	1.91	0.0048	400	16,000	16	2.5

3F	1.91	0.0038	500	20,000	20	2
3G	1.91	0.0032	600	24,000	24	1.66
3H	1.91	0.0027	700	28,000	28	1.43
3A	1.91	0.0024	800	32,000	32	1.25
3A BIS	1.91	0.0024	800	170,667	32	6.66

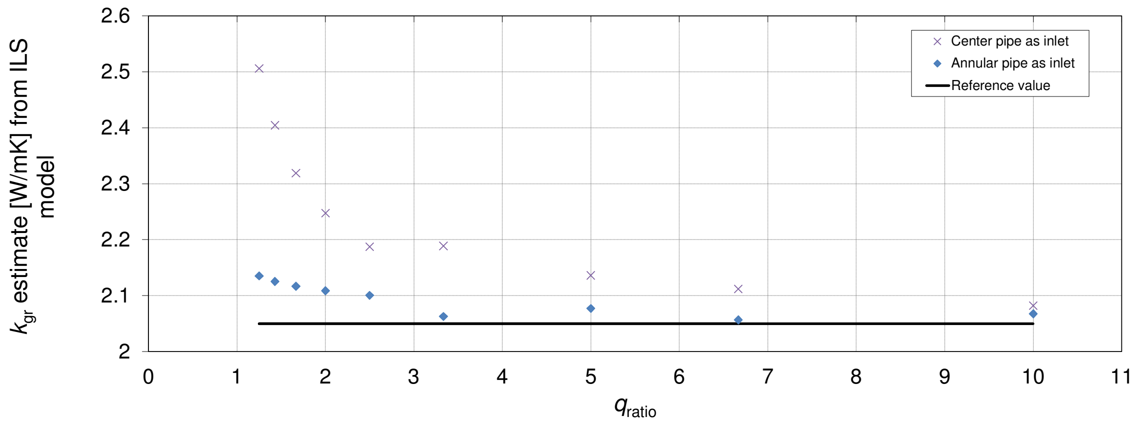

Figure 11: Effective ground thermal conductivity estimation from the FOA of the ILS model compared to the reference value (the results at a different $\frac{\dot{m}}{H}$ value for each case).

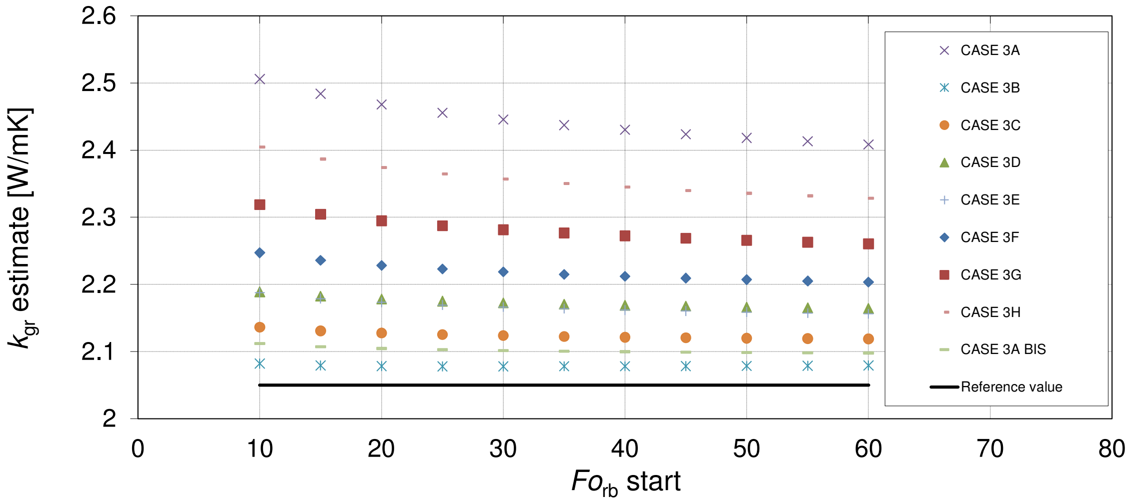

Figure 12: Effective ground thermal conductivity from the ILS model as estimated for different Fo_{rb} windows for the center inlet configuration (the results at a different $\frac{\dot{m}}{H}$ value for each case).

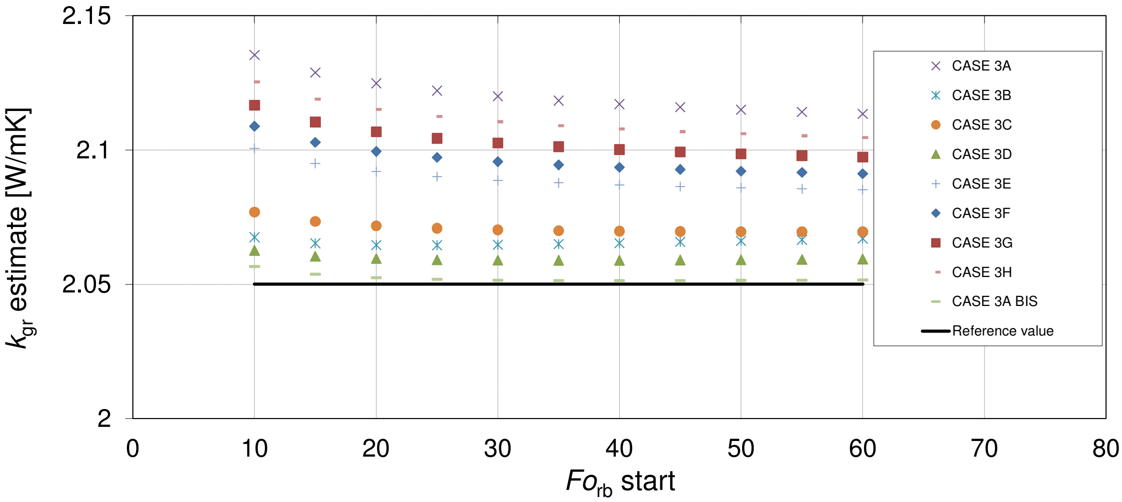

Figure 13: Effective ground thermal conductivity from the ILS model as estimated for different Fo_{rb} windows for the annular inlet configuration (the results at a different $\frac{\dot{m}}{H}$ value for each case).

Figures 8 and 11 show that the parameter q_{ratio} is an indicator of when the effective k_{gr} departs from the thickness-weighted average of the layers' k_{gr} values. For shallow boreholes and large q_{ratio} the ILS estimate is near the weighted average. As q_{ratio} decreases the departure increases as illustrated in Figures 8 to 13. For simplicity, the value of $q_{ratio} = 1$ is a tempting value to choose as the dividing value for when k_{gr} departs from the weighted-thickness average. Identifying an exact value of q_{ratio} for the transition may be difficult because the regions of transition change somewhat depending on the choice of the $\frac{\dot{m}}{H}$ and $\frac{r_b}{H}$ specific values. A departure of 10% is for q_{ratio} included between 2 and 2.5 for the coaxial center-pipe inlet cases considered and the departure increases with decreasing q_{ratio}. The original definition of q_{ratio} expressed by Eq. (1) proves that q_{ratio} is not sensitive of the $\frac{r_b}{H}$ variation. Additional simulations verify that varying $\frac{r_b}{H}$ has little influence on the k_{gr} ILS estimation.

A new cluster of simulations varying $\frac{r_b}{H}$ demonstrates that the influence of the value assumed by q_{ratio} on the ILS-based k_{gr} estimation has more weight than the one due to the specific value assumed by $\frac{r_b}{H}$. In the new cluster of simulations, the $\frac{r_b}{H}$ value has been varied from the value reported in Table 1 (r_b has increased from 0.07 m to 0.14 m). For the sake of brevity, the graphs reporting the results of this simulations cluster have not been reported since their trends are very similar, especially for what concerns Figures 8 and 11. The simulation results highlight that the ILS-based k_{gr} estimations are sensitive mainly to the value related to q_{ratio} regardless of the specific value assumed by the $\frac{r_b}{H}$ ratio. The $\frac{r_b}{H}$ is likely to have a minor influence on the ILS model estimate of the effective ground thermal conductivity. The $\frac{r_b}{H}$ ratio enters the problem when the borehole is treated with a finite length and/or multiple boreholes interacting with each other. The typical duration of TRTs is too short for axial heat conduction in the ground and the finite length to have significant effects. Therefore, any change of $\frac{r_b}{H}$ has little effect on the estimate of k_{gr}.

The results reported in the present section related to the coaxial cases have been graphically explained and clarified also in terms of $g_{0,j}(\tau)$ functions. The condition related to q_{ratio} >>1 has to be satisfied in an ILS-based TRT analysis in order to override the natural heat input rate related to the $g_{0,j}(\tau)$ functions. This makes the ILS-based k_{gr} estimation not sensitive to the effect related to the geothermal gradient incorporated into the $g_{0,j}(\tau)$ functions, therefore closer to the mean k_{gr} value regardless of the k_{gr} variations among the layers. The g_j - function approach of the present study has been applied in the case of a ground characterized by multiple layers of equal thickness with different thermal conductivity values imposed along the depth and corresponding geothermal gradients. Recall that the inlet and outlet temperature profiles in Figures 14 and 16 decrease with time because are related to TRTs in heat extraction mode. Figures 14, 15, 16 and 17 compare the $g_{0,j}$ curves related to two different cases of different H active depths (800 m and 100 m related to the center-inlet CASE 3A and 3B respectively), thus of extremely different q_{ratio} (respectively the lowest and the highest among the multilayered cases considered). In particular, the $g_{0,j}$ curves related to different nodes placed in the annulus at different depths have been compared while the ground thermal conductivity in the corresponding layer still follows the value reported in Table 4. This would make the approach related to the $g_{0,j}(\tau)$ functions analysis feasible also for DTRT analysis. The node numbered 87 is placed in the annulus and is related to the depth of 94.50 m and 11.81 m for CASE 3A and 3B respectively. The node numbered 107 is placed in the annulus and is related to the depth of 304.50 m and 38.06 m for CASE 3A and 3B respectively. The node numbered 127 is placed in the annulus and is related to the depth of 514.50 m and 64.31 m for CASE 3A and 3B respectively. The node numbered 147 is placed in the annulus and is related to the depth of 724.50 m and 90.56 m for CASE 3A and 3B respectively.

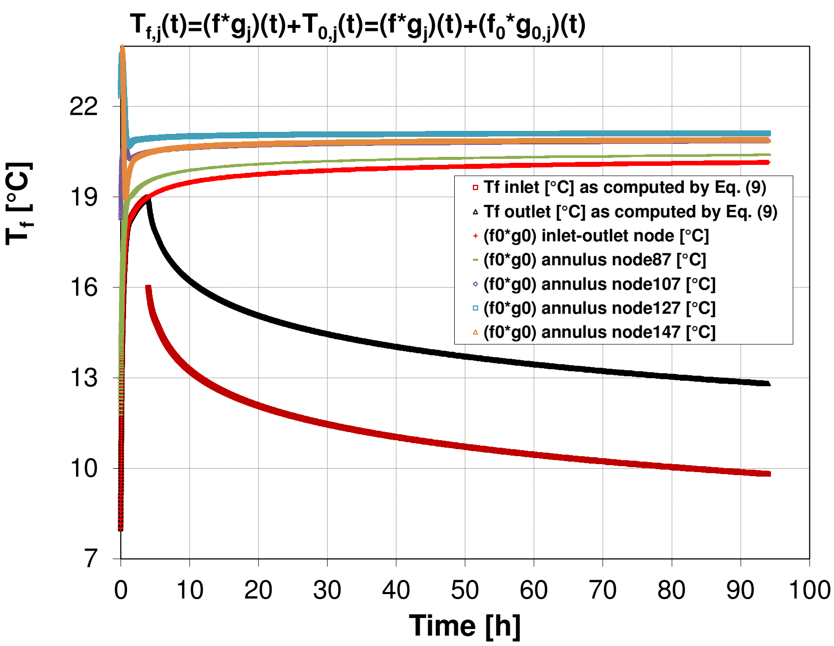

Figure 14: Fluid temperature inlet-outlet from the superposition of the $(f{*}g_j)(\tau)$ and the $(f_0{*}g_{0,j})(\tau)$ convolution products and the $T_{0,j}(\tau)$ profiles for the 4 nodes placed in the annulus at different depths related to the Center inlet Coaxial 800 m DBHE (CASE 3A).

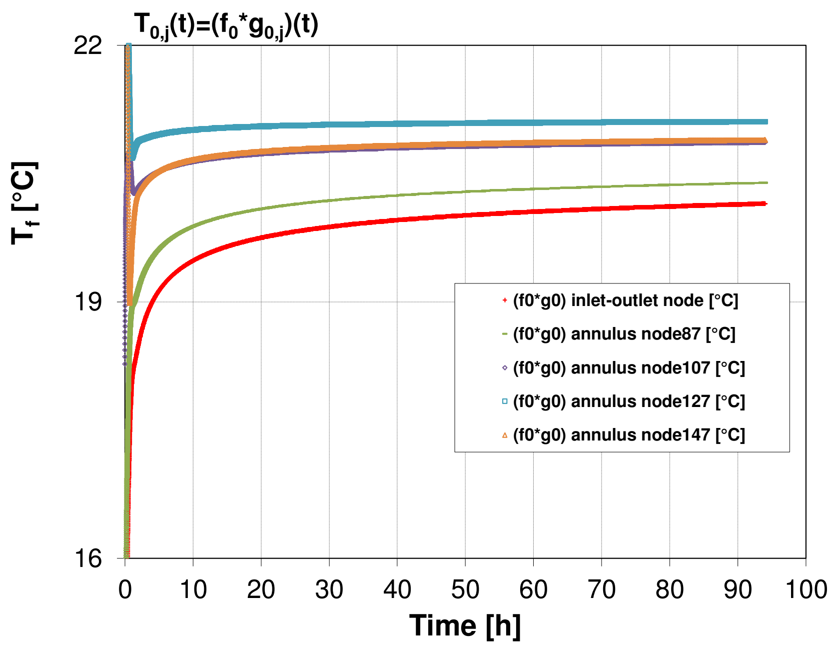

Figure 15: Focus on the $T_{0,j}(\tau)$ related to the inlet and outlet nodes and the 4 nodes placed in the annulus at different depths related to the Center inlet Coaxial 800 m DBHE (CASE 3A).

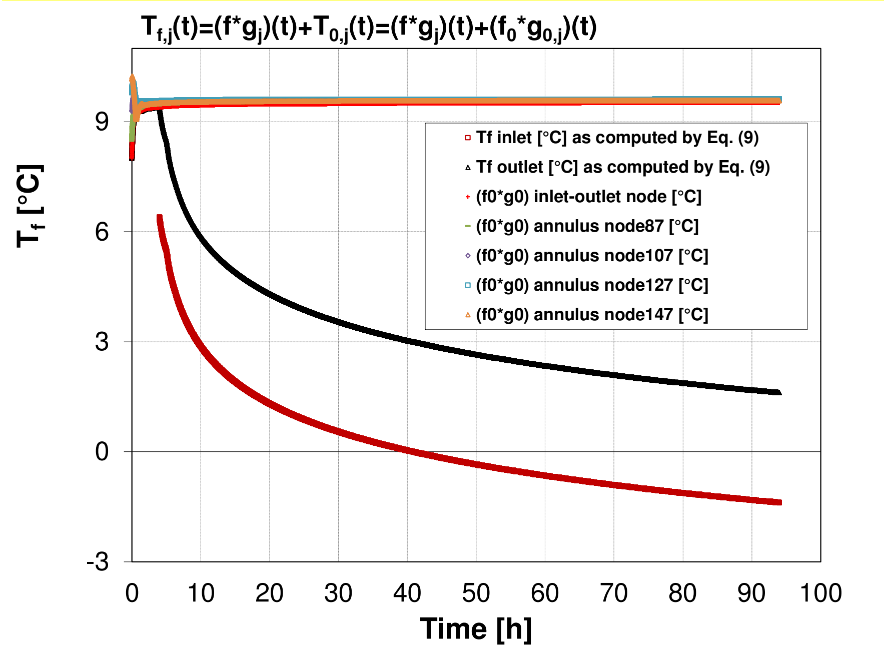

Figure 16: Fluid temperature inlet-outlet from the superposition of the $(f{*}g_j)(\tau)$ and the $(f_0{*}g_{0,j})(\tau)$ convolution products and the $T_{0,j}(\tau)$ profiles for the 4 nodes placed in the annulus at different depths related to the Center inlet Coaxial 100 m BHE (CASE 3B).

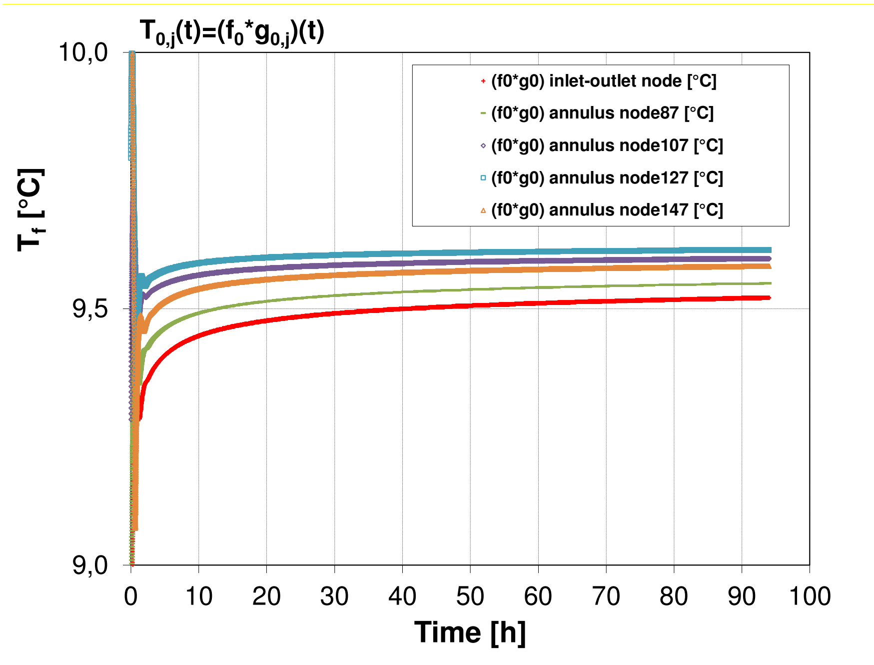

Figure 17: Focus on the $T_{0,j}(\tau)$ profiles related to the inlet and outlet nodes and the 4 nodes placed in the annulus at different depths related to the Center inlet Coaxial 100 m BHE (CASE 3B).

The graphs reported in Figures 14, 15, 16 and 17 compare the $g_{0,j}$ curves related to two different cases of different H active depths (extremely different q_{ratio}, 1.25 and 10 for the CASE 3A and CASE 3B respectively). The $g_{0,j}$ curves related to the inlet and outlet nodes for each same case are necessarily identical. Similarly to Figure 2 for the single-layer subsurface case, the results reported in Figures 14, 15, 16 and 17 for the multilayer case clearly show that the $T_{0,j}(\tau)$ profile related to the center inlet configuration of the coaxial 800 m (q_{ratio} = 1.25) center inlet CASE 3A changes much more at late times than the $T_{0,j}(\tau)$ profiles related to the coaxial 100 m (q_{ratio} = 10) center inlet CASE 3B. Therefore, especially for the coaxial BHE, the $g_{0,j}$ functions can be used as an indicator similar to the one represented by q_{ratio} also in the case of multiple ground layers ($g_{0,j}$ functions and q_{ratio} are directly linked, being affected both by the geothermal gradient $dT_{gr,\infty}/dz$). In particular, the condition related to $q_{ratio} >> 1$ has to be satisfied in an ILS-based TRT and DTRT analysis in order to override the additional available heat input rate related to the $g_{0,j}$ (τ) functions. This makes the ILS-based k_{gr} estimation not sensitive to the effect related to the $g_{0,j}(\tau)$ functions, therefore closer to the mean k_{gr} value regardless of the k_{gr} variations among the layers.

5. Conclusions

In the present study, the modeling of shallow and Deep BHEs with a geothermal gradient in cases of single and multiple layers of different ground thermal conductivities imposed along the depth has been conducted. In particular, a sensitivity analysis on how specific parameters affect the k_{gr} estimation when the FOA of the ILS model is applied to interpret the TRT data. To this aim, three in-house built Fortran90 codes implementing the FD Models related to coaxial, single and double U-BHE geometries have been exploited to evaluate the dimensionless g-transfer functions related to each fluid volume. A suitable spectral method based on the use of the FFT technique and implemented in another dedicated Fortran90 program allows the reconstruction of the fluid temperature profiles computed by the FD Model. The reconstruction of the fluid temperature profiles is obtained by superposing two separated convolutions in the time domain for the entire simulated TRT and serves as the validation of the method. The present method verifies that q_{ratio} is the dominant parameter when the ILS model is used to estimate the effective k_{gr} in TRT data analysis. The conclusions of this study are the following.

1. When q_{ratio} is lower than 1, the $g_{0,j}(\tau)$ function is able to modify the slope of the general solution $T_{f,j}(\tau)$ for each fluid node. The $g_{0,j}(\tau)$ function incorporates the geothermal gradient and can influence the k_{gr} estimation when the ILS model is employed in the TRT analysis.
2. The investigation at $q_{ratio} < 1$ graphically confirms that, as opposed to the coaxial cases, the U-pipes are less influenced by the absolute value of q_{ratio} when the ILS model is used for the ground thermal conductivity estimation from TRT data.
3. In a single-layer subsurface when the geothermal gradient is 0.0 K/m, the nil contribution of additional heat input rate related to the available geothermal heat flux within the BHE length H assures that the k_{gr} can be correctly estimated from the ILS model. For the coaxial

case and geothermal gradient 0.0 K/m, the ILS-based k_{gr} estimations are very close to each other (regardless of the choice of the hydraulic configuration).

4. In the case of a single-layered subsurface, the condition related to q_{ratio} >>1 assures the correct ILS-based k_{gr} estimation for any BHE geometry and hydraulic configuration.

5. In the case of the coaxial center-pipe inlet case with a single-layered subsurface and q_{ratio}<1, the ILS-based k_{gr} estimation when the g_0-function is taken into account can differ by -14 % from the correct ILS-based k_{gr} estimation without taking into account the g_0-function.

6. The q_{ratio} is the dominant parameter when the ILS model is used to estimate the ground thermal conductivity, also in presence of different ground layers of equal thickness with different thermal conductivity values imposed along the depth. Any changes in the r_b/H and $\dot{m}/H$ ratios are not able to mitigate the influence related to the q_{ratio} parameter on the ground thermal conductivity estimation when the ILS model is employed.

7. In the case of a multilayered subsurface, the results for the coaxial BHEs indicate that as q_{ratio} decreases the ILS-based k_{gr} estimation departs from the arithmetic average. The simulations demonstrate that when a strong geothermal gradient exists the difference between the ILS-based k_{gr} estimation and the mean k_{gr} tends to decrease as the total depth decreases. The parameter q_{ratio} is an indicator of this difference. The q_{ratio} parameter indicates when the effective k_{gr} estimated by the ILS model departs from the weighted-thickness average. A departure of 10% is for q_{ratio} included between 2 and 2.5 for the coaxial center-pipe inlet cases considered and the departure increases with decreasing q_{ratio}.

8. In presence of different ground layers of equal thickness with different thermal conductivity values imposed along the depth and corresponding geothermal gradients, the condition related to q_{ratio} >>1 has to be satisfied in an ILS-based TRT analysis in order to override the additional heat input rate (particularly prominent for coaxial DBHEs) provided and incorporated into the $g_{0,j}(\tau)$ functions thus obtaining the ILS-based k_{gr} estimation moving closer to the mean k_{gr} value among the layers. For the coaxial BHEs, the estimated k_{gr} from the ILS model moves closer to the mean k_{gr} value among the layers only if q_{ratio} >>1 regardless of the k_{gr} variations among the layers. The simulations demonstrate also that the cases with the annulus as the inlet have significantly smaller deviations from the average k_{gr}. The errors in the line-source estimates of the mean k_{gr} are expected to be in general less also for single and double U-tube configurations for ground with layers of equal thickness.

9. The g_j - function approach has been applied in the case of a ground characterized by multiple layers of equal thickness with different thermal conductivity values imposed along the depth and corresponding geothermal gradients. This would demonstrate how the approach related to the $g_{0,j}(\tau)$ functions analysis can be feasible also for DTRT analysis.

10. For the coaxial BHE, the $g_{0,j}$ functions can be used as an indicator similar to the one represented by q_{ratio} also in the case of multiple ground layers. In particular, the condition related to q_{ratio} >>1 has to be satisfied in an ILS-based TRT and DTRT analysis in order to override the additional available heat input rate related to the $g_{0,j}$ (τ) functions. This makes the ILS-based k_{gr} estimation not sensitive to the effect related to the $g_{0,j}(\tau)$ functions, therefore closer to the mean k_{gr} value regardless of the k_{gr} variations among the layers.

The present study is the first that highlights the generalization provided by Eq.(9), where the term $T_{0,j}(\tau)=(f_0*g_{0,j})(\tau)$, contrary to T_0 in Eq. (8), is not necessarily constant and the geothermal gradient is taken into account. The present paper could represent the basis for further studies on deconvolution techniques in the time domain aimed to evaluate the g_0 function from any TRT recorded data in order to understand how the g_0 function weights its influence on the ILS-based k_{gr} estimations from a TRT analysis for single and multiple ground layers. The evaluation and removal of the g_0 function from any TRT recorded data through deconvolution techniques (or simply by performing a real complete test of the same duration of the TRT with no heat input rate and only fluid circulation, recording the data, and then detracting these data from the heat injection/extraction TRT) will be of great importance in order to remove the geothermal gradient influence (that is particularly prominent when q_{ratio} <1) and obtain the correct k_{gr} estimations from any TRT analysis based on the ILS model (for single and multiple ground layers).

Acknowledgments

Dr. Morchio acknowledges Polytechnique Montréal and Professor Philippe Pasquier in particular for his visiting period at Polytechnique Montréal during the year 2022.

Appendix A. The thermal response test data analysis with the Infinite line-source (ILS) model

Among the different models that can be applied for achieving the k_{gr} estimation from a TRT, the present study is focused on the ILS model [22,42] which is the first and the simplest for estimating k_{gr}. The ILS model involves the following main assumptions: a constant heat transfer rate in time and space from a linear source, pure heat conduction in an infinite medium, and uniform ground thermal properties. The temperature variation at a point located at a distance r of an infinite linear source that injects (or absorbs) a constant heat transfer rate per unit length $\dot{Q}'$ into an infinite medium in which is embedded is given by:

$$T(r,\tau) - T_{gr,\infty} = \frac{\dot{Q}'}{4\pi k_{gr}} \int_x^\infty \frac{e^{-\beta}}{\beta} d\beta = \frac{\dot{Q}'}{4\pi k_{gr}} E_1(x) \quad \text{(A.1)}$$

where:

$$\dot{Q}' = \frac{\dot{Q}}{H} \quad \text{(A.2)}$$

$$x = \frac{1}{4Fo_r} \quad \text{(A.3)}$$

The thermal equilibrium temperature $T_{gr,\infty}$ between the fluid and the surrounding ground reached at the end of the circulation period prior to the start of heat injection (or extraction) of a TRT, according to the ILS model, is assumed to be the mean value along the BHE active depth H of the undisturbed ground temperature.

The definition of the Fourier number based on the radial coordinate Fo_r is:

$$Fo_r = \frac{\alpha_{gr}\tau}{r^2} \quad \text{(A.4)}$$

In the TRT analysis, the medium is represented by the ground while k_{gr} and α_{gr} are the ground thermal conductivity and diffusivity respectively, τ is the time coordinate. The exponential integral expression $E_1(x)$ can be suitably evaluated by formulas or its convergent series expansion. The polynomial expressions presented by Abramowitz and Stegun [43] represent an accurate approximation of $E_1(x)$ within 1% for Fo_r higher than 0.145 according to Fossa [44]. Among the different series expansions to approximate $E_1(x)$, the expression as truncated at the logarithmic term is the most common:

$$E_1(x) \approx -\gamma - \ln(x) \quad \text{(A.5)}$$

where γ is the Euler constant, $\gamma \approx 0.5772$.

Assuming a 2-resistances model (ground and borehole thermal resistances in series) by introducing the effective borehole resistance, R^*_b, to the right-hand side of Eq. (A.1) and exploiting the approximation in Eq. (A.5), it can be easily demonstrated that the time-varying average fluid temperature (as computed at the inlet and outlet section of the TRT-machine), $T_{f,ave}$, is:

$$T_{f,ave}(\tau) = T_{gr,\infty} + \dot{Q}'\left[R_b^* + \frac{1}{4\pi k_{gr}} E_1\left(\frac{1}{4Fo_{rb}}\right)\right] = T_{gr,\infty} + \dot{Q}'\left\{R_b^* + \frac{1}{4\pi k_{gr}}\left[-\gamma - ln\left(\frac{1}{4Fo_{rb}}\right)\right]\right\} \quad \text{(A.6)}$$

where:

$$T_{f,ave}(\tau) = \frac{[T_{f,in}(\tau) + T_{f,out}(\tau)]}{2} \quad \text{(A.7)}$$

It can be easily demonstrated that Eq. (A.6) can be rearranged assuming the linear form in a semilogarithmic time scale expressed by Eq. (A.8). In this form, Eq. (A.8) is referred to as the simplified line-source model (FOA of the ILS model):

$$T_{f,ave}(\tau) = mln(\tau) + b \quad (A.8)$$

where m is the logarithmic slope and the constant b contains R^*_b. The k_{gr} value is estimated from computing the slope m inside an appropriate Fo_{rb} window ($Fo_{rb} \geq 10$, according to Eskilson [38]):

$$k_{gr} = \frac{\dot{Q}'}{4\pi m} \quad (A.9)$$

For the sake of completeness, it has to be highlighted that in a TRT analysis with the ILS method, the effective borehole thermal resistance R^*_b (in turn related to k_{gr}) is usually calculated after the k_{gr} has been estimated according to the following expression:

$$R_b^*(\tau) = \frac{[T_{f,ave}(\tau) - T_{gr,\infty}]}{\dot{Q}'} - \frac{1}{4\pi k_{gr}}\left[-\gamma - ln\left(\frac{1}{4Fo_{r_b}}\right)\right] \quad (A.10)$$

References

[1] IEA. Heat Pumps; IEA: Paris, France, 2020; Available online: https://www.iea.org/reports/heat-pumps.

[2] B. Köhler, J. Dengler, A. Dinkel, M. Azam, D. Kalz, P. Bonato, F. Tobias, J. Steinbach, M. Ragwitz, M. Arens, A. Aydemir, R. Elsland, C. Frassine, A. Herbst, S. Hirzel, M. Krail, M. Reuter, F. Toro, M. Rehfeldt, M. Jakob. (2016). Mapping and analyses of the current and future (2020-2030) heating/cooling fuel deployment (fossil/renewables) Work package 2: Assessment of the technologies for the year 2012. 10.13140/RG.2.2.28214.96329.

[3] H. Holmberg, J. Acuña, E. Næss, O.K. Sønju, Thermal evaluation of coaxial deep borehole heat exchangers, Renewable Energy (2016), https://doi.org/10.1016/j.renene.2016.05.048.

[4] S. Morchio, M. Fossa, Thermal modeling of deep borehole heat exchangers for geothermal applications in densely populated urban areas, Thermal Science Engineering Progress 13 (2019), https://doi.org/10.1016/j.tsep.2019.100363.

[5] J.W. Deng, Q.P. Wei, M. Liang, S. He, H. Zhang, Field test on energy performance of medium-depth geothermal heat pump systems (MD-GHPs), Energy and Buildings 184 (2019) 289–299. https://doi.org/10.1016/j.enbuild.2018.12.006.

[6] G. Hellström, Borehole Heat Exchangers: State of the Art 2001. Implementing Agreement on Energy Conservation through Energy Storage: Annex 13-Design, Construction and Maintenance of UTES Wells and Boreholes. Subtask 2, International Energy Agency (IEA), 2002.

[7] J. Acuña, Distributed Thermal Response Tests – New Insights on U-pipe and Coaxial Heat Exchangers in Groundwater-filled Boreholes (Thesis (PhD)) KTH Royal Institute of Technology, Stockholm, Sweden, 2013.

[8] S. Morchio, M. Fossa, R. A. Beier, Study on the best heat transfer rate in Thermal Response Test experiments with coaxial and U-pipe Borehole Heat Exchangers. Appl. Therm. Eng. 2022, 200, 117621. [CrossRef]

[9] P. Mogensen, Fluid to duct wall heat transfer in duct system heat storages, in: Proceedings of the International Conference on Subsurface Heat Storage in Theory and Practice, Swedish Council for Building Research, Stockholm, Sweden, June 6-8, 1983, pp. 652-657.

[10] C. Eklöf, S. Gehlin, TED—A Mobile Equipment for Thermal Response Test. Master's Thesis, Lund University, Lund, Sweden, 1996.

[11] W.A. Austin, Development of an in Situ System for Measuring Ground Thermal Properties. Ph.D. Thesis, Oklahoma State University, Stillwater, OK, USA, 1998.

[12] S. Gehlin, Thermal Response Test: Method Development and Evaluation. Ph.D. Thesis, Luleå Tekniska Universitet, Luleå, Sweden, 2002.

[13] S. Morchio, M. Fossa, A. Priarone, A. Boccalatte, Reduced Scale Experimental Modeling of Distributed Thermal Response Tests for the Estimation of the Ground Thermal Conductivity. Energies 2021, 14, 6955. https://doi.org/10.3390/en14216955

[14] J. Acuña, P. Mogensen, B. Palm, Distributed Thermal Response Test on a U-Pipe Borehole Heat Exchanger. In Proceedings of the Effstock 2009, 11th International Conference on Thermal Energy Storage, Stockholm, Sweden, 14–17 June 2009.

[15] J. Acuña, B. Palm, A novel coaxial borehole heat exchanger: description and first distributed thermal response test measurements, in: Proceedings of the World Geothermal Conference, Bali, Indonesia. April 25-2, 2010.

[16] J. Acuña, B. Palm, Distributed thermal response tests on pipe-in-pipe borehole heat exchangers, Applied Energy 109 (2013) 312-320. https://doi.org/10.1016/j.apenergy.2013.01.024.

[17] H. Fujii, H. Okubo, K. Nishi, R. Itoi, K. Ohyama, K. Shibata, An improved thermal response test for U-tube ground heat exchanger based on optical fiber thermometers, Geothermics 38 (2009) 399-406. http://www.sciencedirect.com/science/article/pii/S0375650509000340.

[18] Y. Sakata, T. Katsura, K. Nagano. Multilayer-concept thermal response test: Measurement and analysis methodologies with a case study, Geothermics 71 (2018) 178–186. https://doi.org/10.1016/j.geothermics.2017.09.004.

[19] A. Galgaro, P. Pasquier, L. Schenato, M. Cultrera, G. Dalla Santa. (2018). Soil thermal conductivity from early TRT logs using an active hybrid optic fibre system. 1-9. 10.22488/okstate.18.000023.

[20] S. Morchio, M. Fossa, On the ground thermal conductivity estimation with coaxial borehole heat exchangers according to different undisturbed ground temperature profiles, Applied Thermal Engineering, 2020. https://doi.org/10.1016/j.applthermaleng.2020.115198.

[21] S. Morchio, M. Fossa, Modelling and Validation of a New Hybrid Scheme for Predicting the Performance of U-pipe Borehole Heat Exchangers during Distributed Thermal Response Test Experiments, Applied Thermal Engineering, 2020,

https://doi.org/10.1016/j.applthermaleng.2020.116514.

[22] H.S. Carslaw, J.C. Jaeger, 1959. Conduction of Heat in Solids, 2nd ed. Oxford University Press, Oxford, pp. 261–263. 338-339.

[23] J. Liu, F. Wang, W. Cai, Z. Wang, C. Li, 2020. Numerical investigation on the effects of geological parameters and layered subsurface on the thermal performance of medium-deep borehole heat exchanger. Renew. Energy 149, 384–399. https://www.sciencedirect.com/science/article/pii/S0960148119318609

[24] R.A. Beier, M. Fossa, S. Morchio, 2021. Models of thermal response tests on deep coaxial borehole heat exchangers through multiple ground layers. Appl. Therm. Eng. 184, 116241 https://doi.org/10.1016/j.applthermaleng.2020.116241

[25] A. McDaniel, J. Tinjum, D.J. Hart, Y.F. Lin, A. Stumpf, L. Thomas, Distributed thermal response test to analyze thermal properties in heterogeneous lithology, Geothermics 76 (2018) 116-124. https://doi.org/10.1016/j.geothermics.2018.07.003.

[26] J. Luo, J. Rohn, M. Bayer, A. Priess, W. Xiang, Analysis on performance of borehole heat exchanger in a layered subsurface, Applied Energy 123 (2014) 55-65. https://doi.org/10.1016/j.apenergy.2014.02.044.

[27] S. Signorelli, S. Bassetti. D. Pahud, T. Kohl. Numerical evaluation of thermal response tests, Geothermics 36 (Issue 2) (2007) 141-166. https://doi.org/10.1016/j.geothermics.2006.10.006.

[28] C.K. Lee, Effects of multiple ground layers on thermal response test analysis and ground-source heat pump simulation, Applied Energy 88 (Issue 12) (2011) 4405-4410. https://doi.org/10.1016/j.apenergy.2011.05.023.

[29] C.K. Lee, H.N. Lam, 2012. A modified multi-ground-layer model for borehole ground heat exchangers with an inhomogeneous groundwater flow. Energy 47, 378–387.

[30] J. Raymond, L. Lamarche, 2013. Simulation of thermal response tests in a layered subsurface. Appl. Energy 109, 293–301. http://www.sciencedirect.com/science/article/pii/S0306261913000421.

[31] J. Luo, J. Rohn, W. Xiang, M. Bayer, A. Priess, L. Wilkmann, H. Steger, R. Zorn, 2015. Experimental investigation of a borehole field by enhanced geothermal response test and numerical analysis of performance of the borehole heat exchangers. Energy 84, 473–484. http://www.sciencedirect.com/science/article/pii/S0360544215003035.

[32] Y. Li, X. Han, X. Zhang, S. Geng, C. Li, 2017. Study the performance of borehole heat exchanger considering layered subsurface based on field investigations. Appl. Therm. Eng. 126, 296–304. http://www.sciencedirect.com/science/article/pii/S0360544212007359.

[33] J. Hu, 2017. An improved analytical model for vertical borehole ground heat exchanger with multiple-layer substrates and groundwater flow. Appl. Energy 202, 537–549. http://www.sciencedirect.com/science/article/pii/S0306261917307006.

[34] S. Erol, B. François, 2018. Multilayer analytical model for vertical ground heat exchanger with groundwater flow. Geothermics 71, 294–305. https://doi.org/10.1016/j.geothermics.2017.09.008.S.A.

[35] R.A. Beier, Thermal response tests on deep borehole heat exchangers with geothermal gradient, Appl. Therm. Eng. 178 (2020) 115447, https://doi.org/10.1016/j.applthermaleng.2020.115447.

[36] R.A. Beier, S. Morchio, M. Fossa, Thermal response tests on deep boreholes through multiple ground layers, Geothermics 101 (2022), 102371.

[37] H. Holmberg, R.K. Ramstad, M.H. Riise, Temperature profile measurements - easy, cheap and informative, IGSHPA Research Track Stockholm September 18-20, 2018. https://doi.org/10.22488/okstate.18.000027.

[38] P. Eskilson, Thermal Analysis of Heat Extraction Boreholes, Ph.D. Thesis Lund University of Technology, Sweden, 1987.

[39] D. Marcotte, P. Pasquier, Fast fluid and ground temperature computation for geothermal ground-loop heat exchanger systems, Geothermics 37 (6) (2008) 651e665.

[40] P. Pasquier, D. Marcotte, Efficient computation of heat flux signals to ensure the reproduction of prescribed temperatures at several interacting heat sources, Applied Thermal Engineering, Volume 59, Issues 1–2, 2013, Pages 515-526, ISSN 1359-4311, https://doi.org/10.1016/j.applthermaleng.2013.06.018.

[41] P. Pasquier, D. Marcotte, Joint use of quasi-3D response model and spectral method to simulate borehole heat exchanger, Geothermics, Volume 51, 2014, Pages 281-299, ISSN 0375-6505, https://doi.org/10.1016/j.geothermics.2014.02.001.

[42] L.R. Ingersoll, O.J. Zobel, A.C. Ingersoll, Heat conduction with engineering, geological, and other applications, Physics Today (1955), https://doi.org/10.1063/1.3061951.

[43] M. Abramovitz, I. Stegun, Handbook of Mathematical Functions with Formulas, Graphs, and Mathematical Tables, Nat. Bureau of Standards, 1964, pp. 228–233.

[44] M. Fossa, Correct design of vertical borehole heat exchanger systems through the improvement of the ASHRAE method, Science and Technology for the Built Environment, Taylor and Francis Inc., 2016, pp. 1080–1089.

[45] V.J. Lunardini, 1981. Heat Transfer in Cold Climates. Van Nostrand Reinhold Co.,Toronto, Canada.

[46] J. Raymond, Colloquium 2016: Assessment of subsurface thermal conductivity for geothermal applications, Can. Geotech. J. 55 (9) (2018) 1209–1229, https://doi. org/10.1139/cgj-2017-0447.

[47] T. Kohl, Palaeoclimatic temperature signals — can they be washed out? Tectonophysics 291 (1-4) (1998) 225–234, https://doi.org/10.1016/S0040-1951 (98)00042-0.
[48] T. Kohl, Transient thermal effects below complex topographies, Tectonophysics 306 (3-4) (1999) 311–324, https://doi.org/10.1016/S0040-1951(99)00063-3.
[49] S. Huang, M. Taniguchi, M. Yamano, C. Wang, Detecting urbanization effects on surface and subsurface thermal environment — A case study of Osaka, Sci. Total Environ. 407 (9) (2009) 3142–3152.
[50] A. Nguyen, P. Pasquier, D. Marcotte, Borehole thermal energy storage systems under the influence of groundwater flow and time-varying surface temperature, Geothermics, Volume 66, 2017, Pages 110-118, ISSN 0375-6505, https://doi.org/10.1016/j.geothermics.2016.11.002.